ELSEVIER

Contents lists available at ScienceDirect

Acta Biomaterialia

journal homepage: www.elsevier.com/locate/actbio



Full length article

Injectable three-dimensional tumor microenvironments to study mechanobiology in ovarian cancer



Eric N. Horst^a, Caymen M. Novak^b, Kathleen Burkhard^a, Catherine S. Snyder^c, Rhea Verma^a, Darel E. Crochran^a, Izabella A. Geza^a, Wesley Fermanich^c, Pooja Mehta^c, Denise C. Schlautman^c, Linh A. Tran^d, Michael E. Brezenger^a, Geeta Mehta^{a,c,e,f,g,*}

- ^a Department of Biomedical Engineering, University of Michigan, Ann Arbor, MI 48109, United States
- ^b Department of Internal Medicine, Division of Pulmonary, Critical Care and Sleep Medicine, The Ohio State University Wexner College of Medicine, Columbus, OH 43210, United States
- ^c Department of Materials Science and Engineering, University of Michigan, Ann Arbor, MI 48109, United States
- ^d Department of Chemical Engineering, University of Michigan, Ann Arbor, MI 48109, United States
- ^e Macromolecular Science and Engineering, University of Michigan, Ann Arbor, MI 48109, United States
- f Rogel Cancer Center, University of Michigan, Ann Arbor, MI 48109, United States
- g Precision Health, University of Michigan, Ann Arbor, MI 48109, United States

ARTICLE INFO

Article history: Received 30 August 2021 Revised 19 April 2022 Accepted 21 April 2022 Available online 27 April 2022

Keywords:
Hydrogel
Collagen
Interpenetrating network
Agarose
Alginate
Tumor microenvironment
Mechanobiology
Extracellular matrix
Injectable
Cancers
Ovarian cancers

ABSTRACT

Epithelial ovarian cancers are among the most aggressive forms of gynecological malignancies. Despite the advent of poly adenosine diphosphate-ribose polymerase (PARP) and checkpoint inhibitors, improvement to patient survival has been modest. Limited in part by clinical translation, beneficial therapeutic strategies remain elusive in ovarian cancers. Although elevated levels of extracellular proteins, including collagens, proteoglycans, and glycoproteins, have been linked to chemoresistance, they are often missing from the processes of drug- development and screening. Biophysical and biochemical signaling from the extracellular matrix (ECM) determine cellular phenotype and affect both tumor progression and therapeutic response. However, many state-of-the-art tumor models fail to mimic the complexities of the tumor microenvironment (TME) and omit key signaling components. In this article, two interpenetrating network (IPN) hydrogel scaffold platforms, comprising of alginate-collagen or agarose-collagen, have been characterized for use as 3D in vitro models of epithelial ovarian cancer ECM. These highly tunable, injection mold compatible, and inexpensive IPNs replicate the critical governing physical and chemical signaling present within the ovarian TME. Additionally, an effective and cell-friendly live-cell retrieval method has been established to recover cells post-encapsulation. Lastly, functional mechanotransduction in ovarian cancers was demonstrated by increasing scaffold stiffness within the 3D in vitro ECM models. With these features, the agarose-collagen and alginate-collagen hydrogels provide a robust TME for the study of mechanobiology in epithelial cancers.

Statement of significance

Ovarian cancer is the most lethal gynecologic cancer afflicting women today. Here we present the development, characterization, and validation of 3D interpenetrating platforms to shift the paradigm in standard *in vitro* modeling. These models help elucidate the roles of biophysical and biochemical cues in ovarian cancer progression. The agarose-collagen and alginate-collagen interpenetrating network (IPN) hydrogels are simple to fabricate, inexpensive, and can be modified to create custom mechanical stiffnesses and concentrations of bio-adhesive motifs. Given that investigations into the roles of biophysical characteristics in ovarian cancers have provided incongruent results, we believe that the IPN platforms will be critically important to uncovering molecular drivers. We also expect these platforms to be broadly applicable to studies involving mechanobiology in solid tumors.

© 2022 Acta Materialia Inc. Published by Elsevier Ltd. All rights reserved.

E-mail address: mehtagee@umich.edu (G. Mehta).

Corresponding author.

1. Introduction

Ovarian cancer remains the deadliest of all gynecological malignancies [1]. Diagnoses at an advanced disease stage (III or IV) is routine among ovarian cancer cases. Clinically, advanced diagnosis in ovarian cancer is often related to rapid metastasis, transcoelomic routes of dissemination, and lack of early detection techniques [2–6]. Despite conventional trends, the largest clinical trial on ovarian cancers to date, tracking over two hundred thousand woman for up to 16 years, revealed that early detection does not yield significant survival advantage [7]. These findings reiterate metastasis as a fundamental clinical challenge. Moreover, they underline the importance of establishing ovarian cancer-specific *in vitro* models to accelerate the discovery of effective therapeutic strategies and to better understand disease progression.

Proteogenomic data from TCGA and single cell RNA-seq studies indicate that tumor microenvironments (TME) are significant contributors to the poor overall and progression free survival in ovarian cancer patients [8-13]. The TME components which include tumor supporting cells and tumor secreted extracellular matrices (ECM), form complex multifaceted interactions with cancer cells that act to modulate chemoresistance [14-17]. Unfortunately, high level cell-cell and cell-ECM interactions are often omitted in the currently available in vitro model systems [18]. This in turn leads to underrepresented cellular, molecular, and ECM heterogeneity, consequently impacting clinical translation potential [18-21]. Therefore, in this work, we report on the fabrication and characterization of two accessible 3D scaffold platforms that duplicate critical biophysical and chemical signaling present within the ECM of epithelial ovarian cancers. These injectable scaffolds provide tunable stiffness and composition for varied niche environments, optical accessibility, and live-cell retrieval within an inexpensive and physiologically pertinent TME.

Structural and physical changes to the TME are pivotal hallmarks of metastasis, mediating both tumor progression and therapeutic response [15,19,22-27]. In the ovarian TME, tumor supporting cells secrete large quantities of ECM during the process of desmoplasia. Stromal desmoplastic response accompanies tumorigenesis in the majority of solid tumors and is a robust predictor of poor prognosis [20,23,25,26,28,29]. Since a third of ovarian cancers have their highest protein expression in genetic networks relating to ECM and adhesion [23], it is imperative to characterize and investigate the role of ECM in ovarian cancer outcomes. Compositionally, collagen type I and III are the most abundant proteins present within the ovarian stroma [30,31]. However in ovarian cancers, turnover of these fibrous proteins is acutely amplified, with collagen type I in particular being replaced by extensive neoreactive fiber structures [24,32-34]. Desmoplasia stiffens the TME through transcriptional dysregulation and resultant accumulation of ECM proteins [32,35-39]. The average Young's modulus of the ovarian tumor is approximately 5 kPa, but contains discrete regions with moduli ranging from 16 to 35 kPa [40,41]. As a result, collagen scaffolds alone do not replicate the range of stiffness present within the TME. Since matrix stiffness is an important driver for single and collective cancer cell migration [15], scaffold modulus must be considered when modeling ovarian cancers, as we demonstrate in this report.

While the ECM in most tissues of the human body fits the definition of a hydrogel, it exhibits mechanical properties far greater than mono-hydrogels, or hydrogels composed of a single polymer component alone [42,43]. Similar to polymer composites, biological ECM can be classified as a semi-interpenetrating network (semi-IPN) hydrogel [44]. These *in situ* semi-IPN structures are formed when fibrous proteins are cross-linked, bonded, or mixed with high molecular weight molecules (*i.e.* glycosaminoglycans and polysaccharides, such as hyaluronic acid), thereby vastly improv-

ing the mechanical properties of the stroma [43,45]. We hypothesized that ovarian ECM can be modeled by blending two polymer components, collagen type I with natural-derived polysaccharides, agarose or alginate. In order to test this hypothesis, we created specific gelation procedures to form agarose-collagen and alginatecollagen semi-IPN hydrogels for use as *in vitro* ovarian ECM TME models.

The gelation kinetics of agarose, alginate, and collagen comprises simultaneous gelling for both agarose-collagen and alginatecollagen IPNs. This permits both integrated injection molding and cellular encapsulation for use in mechanobiology studies, including bioreactor stimulation, as shown previously [46,47]. Briefly, collagen type I gelation is controlled by the entropy driven nucleation of triple-helical collagen monomers, followed by lateral cross-linking of thin filaments forming fibers that undergo physical entanglement with surrounding matrices. Agarose is a galactopyronase-based linear polysaccharide with a gelling temperature of approximately 35 °C that promotes hydrogen bonding through an ordered coil-helix transition. The gelled agarose forms an isotropic structure with an average pore size of 100 to 300 nm. Meanwhile, alginate is an anionic polysaccharide comprised of β -D-mannuronic acid (M) and α -L-guluronic acid (G) blocks. Gelation in alginate occurs via divalent cation association with preferential binding to co-operative G blocks greater than 20 monomers in length, forming an isotropic structure with pore sizes ranging from 6 to 200 nm [48,49]. While agarose, alginate, and collagen type I have been used to model both cancer and human tissue previously [33,50-59], these IPNs have not been fully characterized within the mechanical profile of epithelial ovarian tumors. Utilizing these polymers to form semi-IPNs, we modeled the ovarian ECM in vitro. Moreover, we investigated the microstructure associated with each polymer component, alongside mechanical properties, including shear modulus (G), porosity (Φ), and permeability (κ). We examined the cellular viability of ovarian cancer cell lines encapsulated in both IPNs for up to 48 h. For the first time, we also demonstrated live-cell retrieval from agarose-collagen IPNs and performed mechanotransduction assays, utilizing correspondent alginate-collagen and agarose-collagen IPN modulus. Insofar as possible, results were compared directly to patient-derived ovarian cancer xenograft tumors.

2. Materials and methods

2.1. Preparation of interpenetrating network hydrogels

Stock solutions of 1%, 2%, and 3% (w/v) agarose (low gelling temperature; Boston Bioproducts, #P730) were prepared in RPMI growth medium (Thermo Fisher Scientific, Waltham, MA), 1% antibiotic/antimycotic (Thermo Fisher Scientific), and 10% fetal bovine serum (FBS; Gemini Bio-Products, West Sacramento, CA). Stock solutions of rat tail, high concentration (10 mg/mL; Ibidi GmbH, #50,204) and low concentration (3 mg/mL; Cultrex, #344,310,001) collagen type I were prepared on ice. For agarose-collagen IPNs, low concentration collagen (for 1 mg/mL) or high concentration (for 2 mg/mL and 3 mg/mL) were combined with 10X Phosphatebuffered saline (PBS; 10% final volume). The solution was then neutralized using 1% (w/v) NaOH (25.4 μ L, 6 μ L, and 9 μ L for 1 mg/mL, 2 mg/mL, and 3 mg/mL, respectively) and incubated on ice for 10 min to control fiber nucleation. Ultra-pure distilled water was added to collagen solutions to reach a final volume of 350 µL. Molten agarose (400 μ L, warm to touch, \sim 40°) was then mixed vigorously with the appropriate collagen solution (with 1000 µL pipettes). If required, cells were added at this step. The IPNs were cooled for approximately 15 min allowing for complete gelation.

All materials associated with alginate-IPNs were obtained from the Sigma-Aldrich Co, unless otherwise stated. Stock solutions of sodium alginate (ISO, Waldo, ME) were prepared at concentrations of 1%, 2%, and 3% (w/v) in Dulbecco's phosphate-buffered saline (DPBS). Collagen solutions were prepared, as previously described, for a final IPN volume of 600 μL . Both the alginate precursor solution (250 μL) and ice-incubated collagen solution were collected (1 mL syringe) and added to the back end of a luer-lock syringe (1 mL). After locking the female connector to the front port of the syringe, the precursor solution was plunged to the top of the connector while avoiding the introduction of air bubbles. If required, cells were added to the top of this syringe. In a second luer-lock syringe, 125 μL of CaSO4 (45 mM in DPBS) was loaded into the top port, avoiding the introduction of air bubbles. The luer-locks were then connected and mixed vigorously (~ 1 min). The plated alginate-IPNs were allowed to gel for 15 min.

2.2. Immunodeficient xenograft model and decellularization of patient-derived xenografts

All animal experiments were conducted in accordance with the NIH Guidelines for the Care and Use of Laboratory Animals and the Institutional Animal Care and Use Committee (IACUC) of the University of Michigan. Patient cells were recovered from tumors after informed consent under approved IRB protocol, following procedures established previously [60,61]. Single cells were obtained from tumors using the tumor cell dissociation kit (Miltenyi Biotech, San Diego CA) following manufacturer's protocols, followed by 40 μ m filtration. The collected cells were recovered by centrifugation and resuspended in a serum free medium. The patient sample utilized in this report was from the abdominal metastases of stage III high grade serous ovarian cancer (Pt412). NOD SCID gamma female mice were purchased from Jackson Laboratories (Bar Harbor, ME), and injected with ovarian cancer spheroids created from patient-derived cells at age 8-12 weeks. The spheroids were initiated with 100 patient-derived cells on a hanging drop plate and allowed to grow for 7 days, as described previously [60,62]. On Day 7, subcutaneous injections were prepared by carefully harvesting 10 spheroids using a pipette, supported within Growth-Factor-Reduced Matrigel (Corning, NY), along with serum-free B27 medium (1:1 ratio). Tumor size was measured once weekly using calipers. Mice were euthanized after humane endpoint of tumor volume of 1500 mm³, and tumors were dissected. Tumors were diced and centrifuged (500 \times g, 11 min), washed in 1X PBS (\times 3), and washed in 1% SDS solution in 1X PBS at room temperature for 48 h, replacing solution every 12 h. The tissue was then treated with 1% Triton X-100 solution in 1X PBS for 60 min before a final wash in 1X PBS (\times 3). Decellularized tumors were utilized for collagen staining and imaging, porosimetry, and ultra-high resolution SEM imaging.

2.3. Cell culture and live-cell retrieval

Human ovarian cancer cell line OVCAR3 cells (ATCC, Manassas, VA, USA) were cultured in 1640 RPMI growth medium supplemented with 1% antibiotic/antimycotic and 10% FBS. Cells were maintained routinely in tissue culture and passaged upon reaching 80% confluency or until ready for use in 3D culture. For all hydrogel studies, cells were collected using 0.25% trypsin-EDTA (Thermo Fisher Scientific), pelleted, resuspended in 75 μ L of RPMI, and embedded into 600 μ L alginate-collagen and 750 μ L agarose-collagen (cell density was 10 million cells/mL, unless otherwise noted; a slightly larger volume of agarose-collagen was used to account for volume loss during gel fabrication and transfer). Cell laden hydrogels were plated in 15 cm tissue culture plates and subsequently cultured at 37 °C and 5% CO2 in serum containing medium. In some instances cell laden hydrogels were manufactured utilizing OVCAR3 cell line stably expressing GFP. Fluorescent

activated cell sorting was then used to separate the GFP+ OVCAR3 compartment from degraded gel debris for downstream analysis. Viral vectors were purchased from Sigma Aldrich and packaged at the University of Michigan Viral Vector Core. Agarase and alginase enzymes were utilized for agarose-collagen and alginate-collagen IPN degradation respectively (Sigma Aldrich, St. Louis, MO). Briefly, for agarose-collagen IPN, the cell laden agarose gel was coarsely minced and moved to 15 mL conical tubes containing RPMI cell growth medium (500 µL) and agarase enzyme (150 U). Hydrogel samples were left submerged in enzyme for approximately 45 min, stirring with a sterile spatula and pipetting (1000 μL pipettes) at 5 min intervals. The final cell slurry was then filtered (100 μm nylon mesh; Thermo Fisher Scientific) into a 50 mL conical tube with 10 mL of fresh medium. The solution was then passed through the same filter (\times 2) before centrifuging (400 \times g) and suspending in fresh cell growth medium. For cell laden alginate-IPNs, hydrogels were scraped into a 50 mL conical tube containing medium (2 mL) and alginase enzyme (50 U). After 15 min, a pipette (1000 μL pipettes) was used to break up the hydrogel into a consistent solution before following the filtration steps above.

2.4. Microscopy and measurement of collagen content

Second harmonic generation (SHG) images were obtained using a Leica SPX8 laser scanning confocal microscope with an excitation wavelength of 860 nm and a collection window of 425 to 435 nm. A 40 \times water emersion lens with a 100 Hz scan speed was utilized to capture z stacks of 1024 \times 1024 pixels (129.17 μ m \times 129.17 μ m) with a 0.5 µm step size and a final z-height of 7.5 µm for each image. Collagen density and fiber spacing analysis were performed using custom Matlab scripts. Briefly, images were thresholded and either fiber area or average fiber intersection to a grid overlay were measured respectively. Hydrogels and decellularized tumors were histologically processed for staining, briefly samples were processed, embedded in paraffin, and sectioned to a thickness of 7.5 µm. Slides were stained with sirius red (Chondrex, Woodinville, WA) and imaged using a Nikon E800 light microscope to visualize collagen content. Live-cell viability imaging was performed using a calibrated inverted microscope (Olympus IX81, Japan, equipped with an ORCA R2 cooled CCD camera and CellSens software). High resolution live-cell imaging was performed using a Leica SPX8 multiphoton laser scanning confocal microscope with a 60 \times oil objective. For live-cell viability studies, 50 µL of hydrogel with 2 million cell/mL were spread thinly across each well of a Millicell EZ 4-well glass slide (Millipore, Burlington, MA), medium was exchanged every 24 h. At the final time point, calcein-AM (0.728 µM; Biotium, #B2261) and ethidium homodimer (1.456 µM; Biotium, #40,010) were added to each well. Fluorescent images were taken following a 10 min incubation.

2.5. Electron microscopy and porosimetry

Hydrogels and decellularized tumors were fixed in 2.5% glutaraldehyde overnight at 4 °C and 1% osmium tetroxide for 1 hour at room temperature prior to dehydration in an ethanol series, critical point drying (Leica EM CPD300), sputter coating with 2–5 nm gold, and then imaged with a TESCAN Mira3 resolution scanning electron microscope at $40,000 \times 16,000 \times 16,$

2.6. Characterization of mechanical properties

Oscillatory rheometry (ARES, TA Instrument, New Castle, DE) was used to determine IPN shear moduli. Tests were performed using a 25 mm parallel plate geometry. Frequency sweeps were performed at 0.5% strain value with frequency ranging from 100 rad/s to 0.1 rad/s derived from the linear portion of strain sweep tests at 0.3 Hz. The storage modulus, G', loss modulus, G'', and resultant complex modulus, G*, were recorded. Poisson's ratio of 0.49 was assumed for the hydrogels and utilized to convert shear modulus to elastic modulus [63–65].

2.7. Flow cytometry sorting and wound healing assay

OVCAR3 cells were sorted for viability after hydrogel degradation using FACS. Briefly, cells were recovered by centrifugation and resuspended in FACS buffer with 300 µmol/L 4',6-diamidino-2phenylindole (DAPI). Cells were processed through a flow cytometer, using forward and side scatter to isolate viable DAPI-negative single cells. Gates were established using 2D tissue cultured OV-CAR3. GFP+ OVCAR3 cells were cultured in IPN hydrogels of varying stiffness for 48 h. Cells were then harvested and sorted by FACS to fully separate the cells from any remaining gel debris (dia. > 100 µm). Cells were then plated in 24-well plates at a density of 300,000 cells/mL for 12 h in serum-containing medium before creating a wound with a 200 µL micropipette tip. Cells were then rinsed with PBS, replaced with serum-starved medium, and returned to the incubator. Fluorescent images at 4 × magnification were taken on an inverted microscope at the 0 hr, 12 hr, 24 hr, and 48 hr time points. Wound edge progression was measured and compared to the initial wound using ImageJ.

2.8. Gene expression analysis

After 48 h in culture, cell laden hydrogels were digested at 4 °C overnight in 1 mL of buffer RLT (with 10% β -Mercaptoethanol). RNA purification was performed using the RNeasy mini kit (Qiagen, #74,106, Germantown, MD) as specified in the manufacturer's protocol. RNA concentrations were determined using a Nanodrop (Nanodrop Technologies, Wilmington, DE). Gene expression was investigated through RT-qPCR for a variety of genes involved in metastasis, Rho/Rock, YAP/TAZ, collagen binding, and MAPK/MEK signaling. Primers utilized for RT-qPCR are tabulated in Supplementary Table S1. RT-qPCR was performed using 96 well plates and Power SYBR Green PCR master mix (Applied Biosystems, ILT4367659, Thermo Fisher Scientific, Waltham, MA) on 7900HT system (Applied Biosystems) through the Advanced Genomics Core at the University of Michigan. The $2^{\Delta\Delta CT}$ method was used to compare the lower (E₁) and higher (E₂) matrix stiffness to the 2D controls. Three to 6 biological replicates per condition were analyzed with three technical replicates per plate.

2.9. Statistical analysis

All data were reported as mean \pm SD of triplicate experiments unless otherwise noted. Differences between groups were compared by the two-tailed Student's (t-test), one-way analysis of variance, or by Mann-Whitney U test and analyzed using GraphPad Prism version 7.0 software (GraphPad Software, San Diego, CA).

3. Results

3.1. Collagen type i is distributed homogeneously in discrete regions of semi-IPNs

To inform key design criteria for the ovarian TME matrices, the material characteristics were compared directly to decellularized patient-derived xenograft tumors (DPDXT; Fig. 1A). Xenografts were produced in immunodeficient mice by subcutaneous injection of patient-derived ovarian cancer spheroids (harvested at day 7). At the humane endpoints, xenograft tumors were collected and decellularized as previously described [66]. For IPN fabrication, agarose-collagen and alginate-collagen were mixed and gelled in glass molds utilizing 3% (w/v) polysaccharide precursor solutions and collagen type I (Fig. 1B). Collagen type I concentration varies between 1 mg/mL to 3 mg/mL within the ovarian TME [50,67,68]. Hence, three collagen concentrations (1 mg/mL, 2 mg/mL, and 3 mg/mL) were synthesized in 3% (w/v) agarose and 3% (w/v) alginate precursor solution to replicate this range *in vitro*, stained with sirius red, and qualitatively compared to DPDXTs.

Collagen fiber analysis was performed on 3% (w/v) precursor alginate and agarose solutions as they had the highest viscosity, and therefore proved most difficult to mix. The polymerization temperature of collagen affects the balance of hydrophobic and electrostatic interactions and hydrogen bonding between collagen monomers and fibrils [69-71]. Lowering the temperature favors lateral fibril and fiber growth. Incubation for 10 min at 0 °C post collagen neutralization was important to generate both a homogenous dispersion of collagen fibers and a larger average fiber diameter. Further, as agarose and alginate polymerize faster than collagen fibers, collagen presented a discontinuous morphology when mixed (Fig. 1C,E). These gelling kinetics are also why agarosecollagen and alginate-collagen hydrogels are classified as simultaneous semi-IPNs. To further characterize the fibrous collagen distribution, we utilized SHG microscopy, imaging the same sample thickness to visualize collagen microstructure in agarose and alginate IPNs (3%), and DPDXTs, respectively (Fig. 1E,F). Homogenous, discrete regions of collagen were visualized in each sample. Collagen fiber area density and average distance between fibers were calculated using a custom MATLAB script (Fig. 1G,H). Collagen fiber area increased stepwise for both IPN systems from 1 to 3 mg/mL collagen. Similarly, average fiber distance decreased with collagen concentration. However, average fiber distance was generally larger in alginate and may be accounted for by differences in thermodynamics and/or mixing protocols (pipette versus syringe). The patient-derived xenograft tumor fiber quantification appeared to most closely resemble IPNs containing 3 mg/mL collagen, although significant differences remain in terms of fiber length and width.

3.2. Semi-IPN ultrastructure demonstrates homogenous porosity and interspersed collagen fibers

In order to compare the *in vivo* tumor ultrastructure to that of semi-IPNs, SEM imaging was conducted. Since SEM imaging at high resolution is incompatible with wet microstructure and nanoarchitecture of the IPN polysaccharide compartment, critical point drying (CPD) was utilized for sample preparation. The fixed DPDXTs and IPN samples of varying alginate and agarose precursor concentrations (1%, 2%, and 3%) were dehydrated via CPD for direct SEM imaging (Fig. 2). Both IPNs displayed muted architecture at the solid gel-air interface, attributed to elevated surface tension during gelation. To avoid imaging at the IPN surface, we fractured the dehydrated hydrogels prior to sputter coating. In accordance with previous literature, ordered fibrous structures were observed within the DPDXTs (Fig. 2A) [24,34]. To demonstrate scale, an ovarian cancer cell was also demarcated in situ (Fig. 2A, far right panel). IPNs at a final collagen concentration of 1 mg/mL were compared to collagen-free agarose and alginate hydrogels (Fig. 2B,C). Thick collagen fibers were visible, interspersed within the web-like tightly packed agarose and alginate hydrogels, and were in agreement with diameters previously observed (Fig. 1). The web-like nature of agarose-collagen IPNs has been reported by others [52,72].

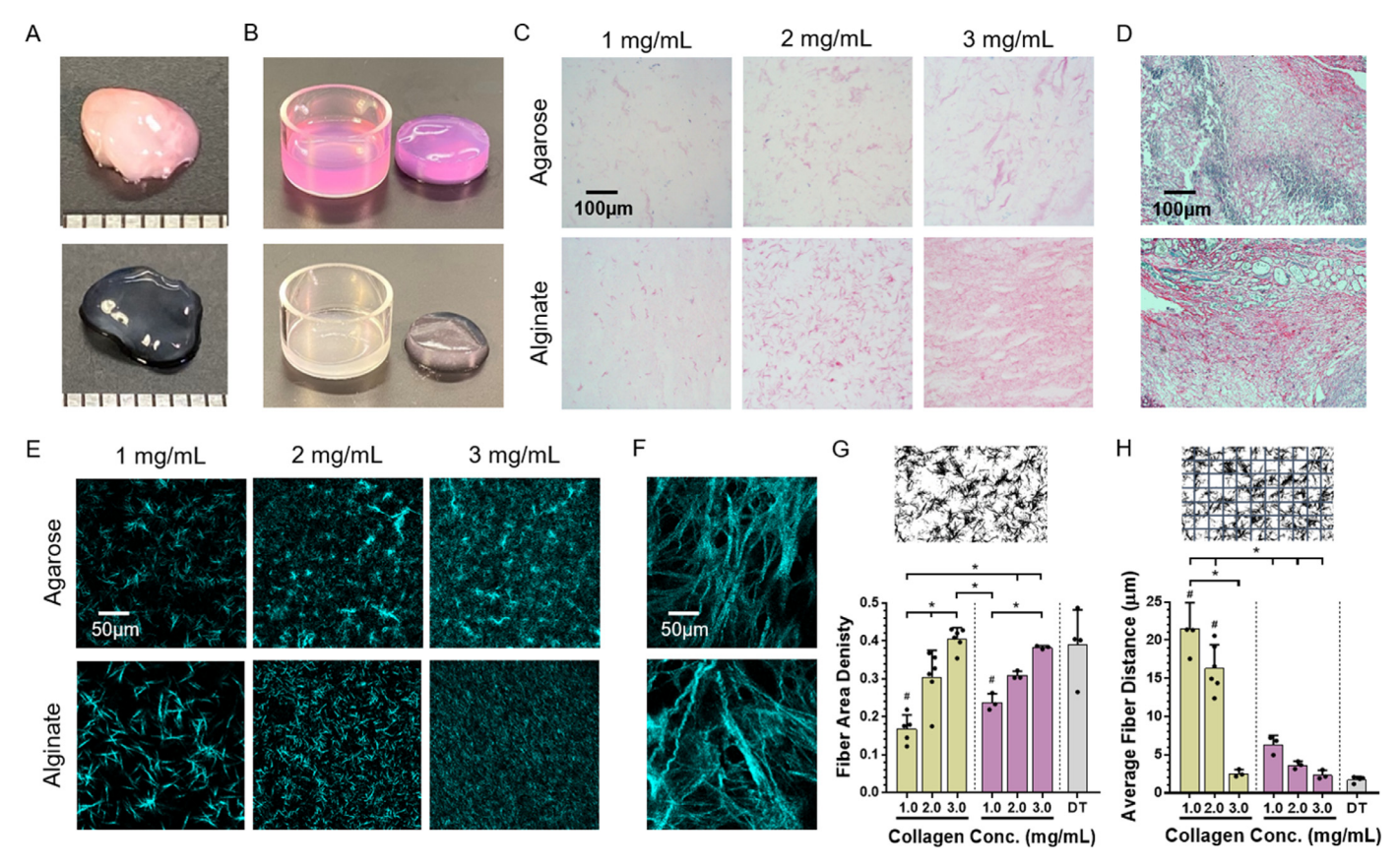


Fig. 1. Collagen formation within semi-interpenetrating network hydrogels. A. Xenograft, ovarian cancer patient derived tumors (top) were decellularized for downstream analysis (bottom). Bar segments = 1 mm. B. Injection molded 3% (w/v) agarose in the presence of 1 mg/mL collagen (top; dark pink) and 3% (w/v) alginate in the presence of 1 mg/mL collagen (bottom; tan). C, D. Histological stains (sirius red) of 3% (w/v) agarose and alginate hydrogels with increasing collagen content (1 mg/mL, 2 mg/mL, and 3 mg/mL) and decellularized tumors (slice thickness = 7.5 μ m). E, F. Second harmonic generation (SHG) imaging of agarose-collagen and alginate-collagen IPNs plus decellularized tumors; reflecting conditions used for histology (sample thickness = 7.5 μ m). G. Quantification of fiber area in SHG images; representative images (top). H. Quantification of average fiber distance in SHG images; representative image threshold plus mesh overlay (top). All data points represent mean \pm SDs with superimposed data points (alginate = tan, agarose = dark pink, decellularized tumors = gray); asterisk and hash-mark denotes significance P < 0.05 compared to decellularized tumors, determined by one-way analysis of variance (ANOVA) followed by post-hoc Mann-Whitney U-tests. (For interpretation of the references to colour in this figure legend, the reader is referred to the web version of this article.)

With pore size measured to be less than 1 μ m, cell mobility would be obstructed in all IPN conditions. While not physiologically accurate, immobilization is a property generally desired in studies involving 3D mechanotransduction [15,46,47]. Likewise, homogenous pore size and distribution (Fig. 2C) allow for excellent load transfer, homogenous fluid perfusion flow, and consistent diffusional characteristics [15].

In addition to SEM, porosity (Φ) and permeability (κ) were measured using a mercury porosimeter. This procedure required large, dehydrated sample volumes (approximately 1.5 cm³ per run) and therefore made the use of CPD unrealistic. We instead employed HMDS dilution series for a cost effective and improved sample turnover rate. Samples were dehydrated via sequential solutions starting with aqueous and proceeding through ethanol (100%), HMDS (100%), and an overnight off-gassing step. CPD was utilized as a gold standard and samples prepared via HMDS were compared directly to those prepared via CPD with SEM (Supplementary Fig. 1). Alginate and 1% (w/v) agarose IPNs did not prepare well with HMDS and were therefore not recorded (data not shown). Relative diffusion rates of 3-5 kDa FITC conjugated dextran were also measured in IPN samples of varying alginate and agarose precursor concentrations (1%, 2%, and 3%) with 1 mg/mL collagen (Supplementary Fig. 2). A ratio of 3-5 to 10 kDa FITC conjugated dextran were measured in the exponential phase of diffusion (hour 3 of the 6 IPN conditioned outlined above) and were normalized to each 1% (w/v) polysaccharide condition respectively (Supplemental Table 2). The porosity and permeability of 2% (w/v) agarose with 1 mg/mL collagen was 46.31 \pm 20.32% and 4.03 \times 10^{-11} \pm 4.06 \times 10^{-11} cm $^{-2}$, respectively, and closely resembled previous literature [73,74]. The porosity and permeability of 3% (w/v) agarose with 1 mg/mL collagen was 55.67 \pm 6.54% and 1.68 \times 10^{-12} \pm 1.23 \times 10^{-12} cm $^{-2}$, respectively, and for DPDXTs was measured as 39.76 \pm 4.89% and 2.58 \times 10^{-11} \pm 2.04 \times 10^{-11} cm $^{-2}$, respectively. Although modest decreases to visual pore size were seen with increased agarose content, they were not recognized by porosimetry. DPDTXs were observed to contain permeability comparable to that of 2% (w/v) agarose with 1 mg/mL collagen. The diminished porosity of the DPDTXs may indicate that the porous nanoarchitecture was somewhat collapsed by HMDS dehydration.

3.3. Semi-IPNs recapitulate the shear moduli of in vivo tumors

To validate that IPN moduli replicated that of the ovarian TME, we began by synthesizing a series of agarose-collagen and alginate-collagen IPNs with fixed collagen concentrations (1 mg/mL). Altering the collagen concentration between 1 mg/mL to 3 mg/mL is not thought to significantly affect the mechanical properties of agarose/collagen and alginate/collagen IPNs within the present range [51,75–77]. Limited by the viscosity of alginate precursor concentrations, 3% (w/v) produced the highest stiffness achievable utilizing luer-lock syringe mixing. Increasing polysaccharide con-

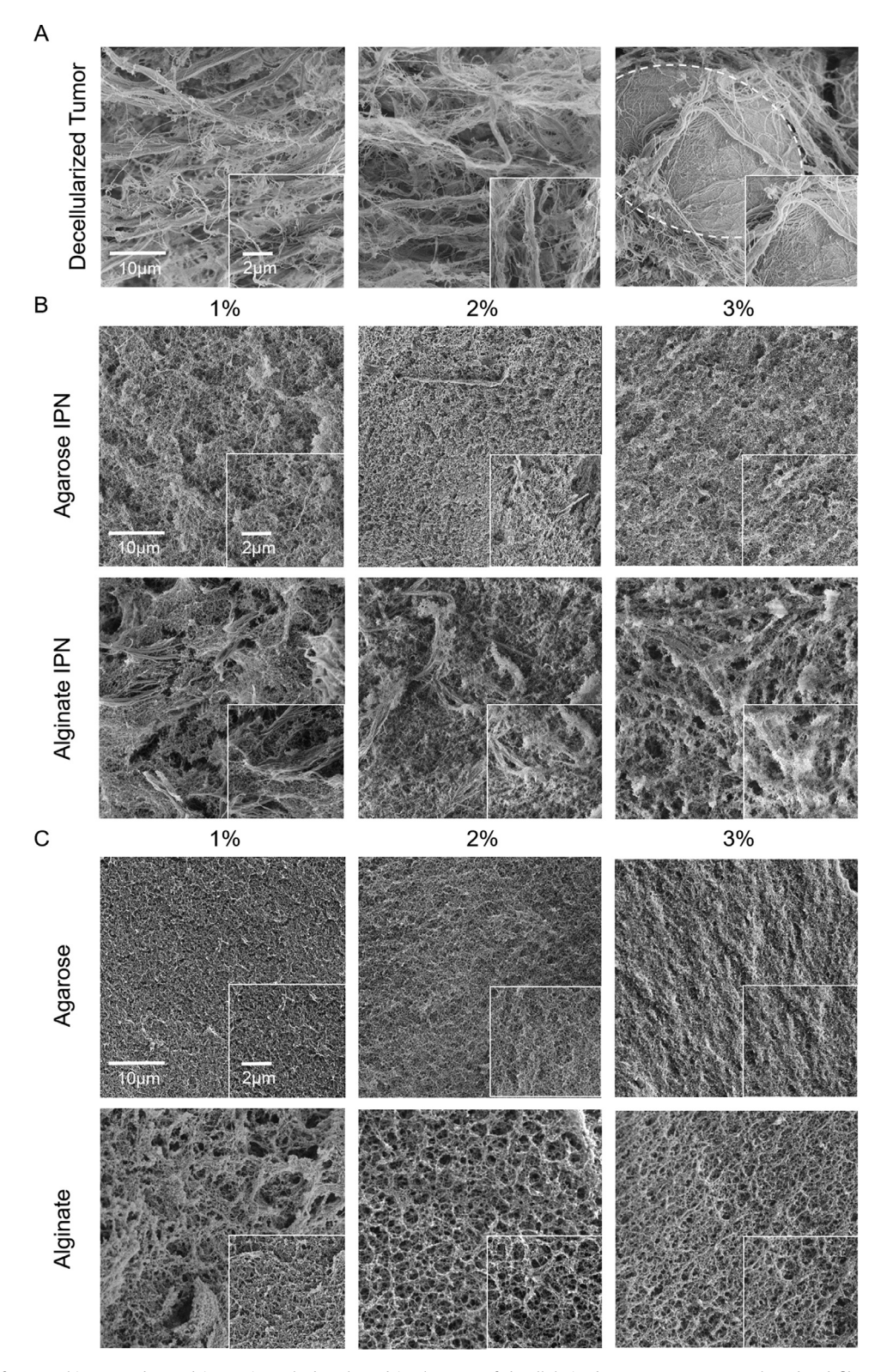


Fig. 2. Comparison of nanoarchitecture observed in semi-IPN hydrogels and in the ECM of decellularized tumors. **A.** SEM reveals ordered fibrous structures throughout decellularized patient derived ovarian cancer xenograft tumors. Left and center panels show two different representative images. Right panel shows an ovarian cancer cell within the matrix. **B.** Thick interpenetrating collagen fibers are observed throughout agarose-collagen and alginate-collagen (1 mg/mL) IPNs (1% to 3% of precursor alginate and agarose; w/v) with dense, well defined pore structure. **C.** Control agarose and alginate hydrogels ranging from 1% to 3% (w/v) without the presence of collagen, demonstrate modest variation of pore size with increased hydrogel content. (For interpretation of the references to colour in this figure legend, the reader is referred to the web version of this article.)

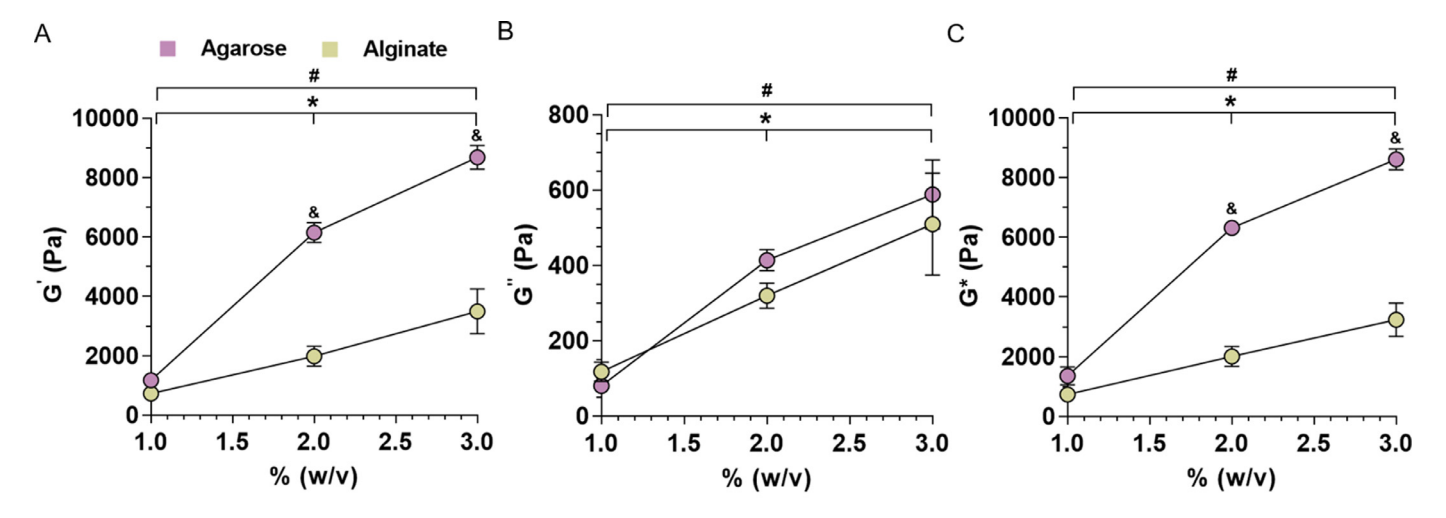


Fig. 3. Rheological analysis of agarose and alginate IPN hydrogels. Parallel-plate rheometric evaluation of: **A.** shear storage modulus (G'), **B.** shear loss modulus (G''), **C.** complex shear modulus (G^*) for 1% (w/v) to 3% (w/v) agarose and alginate hydrogels with 1 mg/mL collagen, for $n \ge 4$. All data points represent mean \pm SDs with superimposed data points (alginate \pm tan, agarose \pm dark pink); asterisk and hash-mark (*, #) denotes significance E'0.01 between conditions of either agarose-collagen or alginate-collagen respectively, while ampersand (&) denotes significance E'0.01 between IPNs, determined by one-way analysis of variance (ANOVA) followed by post-hoc Mann-Whitney E'1 test.

tent yielded stable hydrogels that were measured by parallel plate rheometry. Both IPN systems spanned the average elastic moduli reported in ovarian tumors (5 kPa; Fig. 3). In accordance with previous literature, agarose and alginate IPNs displayed a nearly linear relationship between complex shear modulus and percent weight to volume ratio in this region [78,79]. Complex shear modulus in agarose-collagen hydrogels spanned a 5 fold range, with similar shear moduli previously reported for 1% (w/v) agarose plus 1 mg/mL collagen IPN hydrogels [52].

3.4. Semi-IPNs support live-cell imaging and maintain ovarian cancer cell viability during 3D growth and post cell-retrieval

Beyond replicating the mechanical environment of ovarian tumors, we sought to verify cellular viability and optical accessibility within 3D platform for up to 48 h. To confirm that semi-IPNs can recapitulate ovarian TME, we encapsulated the immortalized high grade serous ovarian cancer cell line, OVCAR3, within 3% agarose or alginate plus 1 mg/mL collagen IPN hydrogels. Live-cell viability was assessed with fluorescent microscopy at the 0, 24, and 48 hour time points using calcein-AM and ethidium homodimer (Fig. 4A). Average cell viability was maintained above 80% for the duration of 48 h in 3D platforms (Fig. 4B). Utilizing high resolution multiphoton microscopy, we verified optical accessibility within agarose and alginate IPN platform systems by observing calcein-AM and ethidium homodimer stained OVCAR3 cells (48 hr; Fig. 4C). We next investigated live-cell retrieval after encapsulation in 3D platform. Live-cell retrieval from agarose hydrogels had been previously considered impossible [80-84]. Using a prolonged agarase enzyme degradation (45 min) in combination with gentle mixing and stirring (5 min intervals), we discovered that encapsulated OV-CAR3 cells were recoverable from agarose-collagen IPN hydrogels. In contrast, the live cells were retrieved from alginate gels using a gentle dissolution strategy. Cell viability was measured via manual cell counting for 1%, 2%, and 3% (w/v) agarose and alginate hydrogel conditions, each displaying an average viability greater than 75% (Supplementary Fig. 3). In situ culture conditions were duplicated for cell-retrieval, whereby hydrogels were degraded, filtered, and sorted via flow cytometry for cellular viability (Fig. 4D), likewise we verified cell retrieval from alginate-collagen encapsulation (Fig. 4D). Retrieved OVCAR3 cells maintained significantly high viability (> 75%), measured via flow cytometry (Fig. 4E). A minor drop in cell viability was observed in agarose hydrogels at the 48 hour time point. To investigate whether this was due to prolonged exposure to the agarase enzyme, we performed a 48 hour study in 2D and found the required enzyme concentration did not significantly impact cellular viability (Supplementary Fig. 4).

3.5. Semi-IPNs support mechanical transduction of ovarian cancer cells

We next investigated whether changes to scaffold stiffness impacted the migrational behavior of OVCAR3. Agarose and alginate hydrogels are generally considered bioinert in ovarian cancer cell models, thus the cells do not directly interact via chemical signaling with these polymers. Physical stimulus are instead transduced from the polysaccharide scaffolding through physical entanglement of collagen fibers via binding motifs (GFOGER, DDR1, and DDR2) [85]. Given that collagen concentration in DPDTXs most closely resembled IPNs with a final concentration of 3 mg/mL (Fig. 1C–H), we chose this collagen content to inform cellular transduction for this study.

Stiffness of alginate and agarose within the present range are orders of magnitude greater than 3D collagen gels alone. Changing collagen content within this range has negligible impact on IPN modulus [51,75-77]. Informed by our investigation into IPN rheometry (Fig. 3), we chose the lowest (E_1) and highest (E_2) possible moduli reproduced by the agarose and alginate IPN gels (Supplementary Fig. 5). The GFP+ OVCAR3 cells were encapsulated in alginate and agarose hydrogels with 3 mg/mL collagen for 48 h. Cells were then recovered, sorted by flow cytometry for GFP expression, and plated on 2D tissue culture plates for migrational assessment via wound healing assay. In order to minimize exposure time with the 2D surface, OVCAR3 cells were placed on 2D for 12 h. Migration was then analyzed for 48 h post-wound, to avoid a reversion of phenotype. Changes in phenotype due to ECM stiffness have been described in a variety of cell types [40,86-91]. Capacity for cellular adherence was also found to be affected by the 3D platforms, and both washing and medium exchange had to be performed with care to avoid shearing-off cells. Cells that had been encapsulated in pliable matrices (E1) took significantly longer to fill the wound in comparison to cells grown on 2D plates (Fig. 5A, B). This effect was abrogated by cells grown in stiffer matrices (E2). As mechanotransduction relating to ovarian TME stiffness is highly

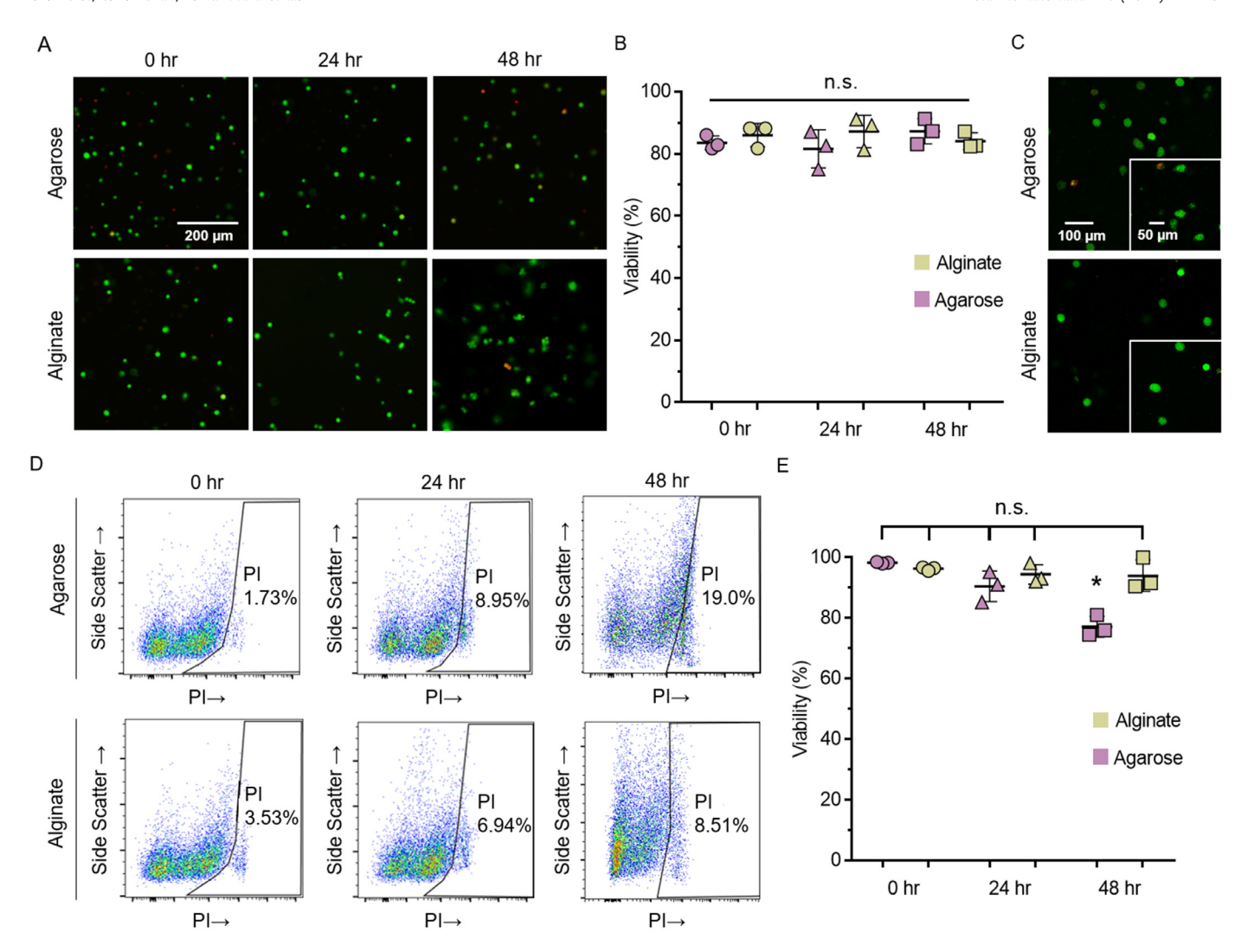


Fig. 4. Optical accessibility, cell viability, and live-cell retrieval from IPN scaffolds. A. OVCAR3 cells were encapsulated in 3% agarose + 1 mg/mL collagen and 3% alginate + 1 mg/mL collagen for 0, 24, and 48 h respectively. Fluorescent images of calcein-AM and ethidium homodimer stained cells were captured using an inverted light microscope. B. In situ cell viability between each condition and time point did not show significance. C. Encapsulated OVCAR3 cells were imaged via multiphoton high resolution microscopy, displaying high degree of optical accessibility. D. OVCAR3 cells were recovered after encapsulation for 0, 24, and 48 h in 3% agarose + 1 mg/mL collagen and 3% alginate + 1 mg/mL collagen. Recovered cells were analyzed for cell viability via flow cytometry. E. Flow-based quantification of recovered cell viability. All data points were plotted (n = 3); asterisk denotes significance P < 0.01 compared to each other condition, determined by ANOVA followed by post-hoc analysis. (For interpretation of the references to colour in this figure legend, the reader is referred to the web version of this article.)

contested *in vitro* [25,40,92–94], we assessed gene expression corresponding to the three contending molecular pathways (YAP/TAZ, Rho/Rock, and MAPK/MEK) (Supplementary Fig. 6). Genes involved in integrins, serpin, and MAPK activation were found to be significantly upregulated in response to stiffer matrix (E_2) (Fig. 6).

4. Discussion

With diverse compartments of acellular and cellular activity, ovarian cancer cells are inundated with a variety of biochemical and biophysical signals [18,27,46,95]. Many of these signals influence cellular phenotype, and when absent from *in vitro* systems prohibit productive clinical translation and drug discovery. While *in vivo* models, such as patient-derived xenografts (PDX) recapitulate many of these stimuli (and are widely considered the gold standard), they are time-consuming and expensive to produce. Comprehensive *in vitro* models are therefore a vital alternative to generate biologically relevant, high-throughput, tunable, and clinically translatable technologies. In this report, we outlined two accessible 3D semi-IPN scaffolds that mimic the material prop-

erties of the ovarian tumor ECM. Inspired by the ECM of the TME, we manipulated the polysaccharide-protein polymer composite hydrogels, agarose-collagen and alginate-collagen, to produce two durable mechanical environments for modeling ovarian TME. Although agarose-collagen and alginate-collagen IPNs are widely used in tissue engineering, a comprehensive characterization appropriate for studying ovarian cancer was critically needed [54,56,57,75,96,97].

Collagen type I is one of the most abundant macromolecules in the ovarian TME [23,26,67,98] and is vital to promoting epithelial to mesenchymal transition (EMT) [24,67,99,100]. During ovarian cancer tumorigenesis, collagen type I is heavily remodeled, whereby thick collagen networks are replaced by uniformly distributed neoreactive fiber structures [33,34]. In cortical inclusion cysts, collagen type I concentrations have been reported as high as 2.1 mg/mL, with similar concentrations utilized to grow ovarian cancer cell lines *in vitro* [50,67]. Emulating this process in semi-IPNs, we generated collagen fibers over a physiologically pertinent range of concentrations. Within this range, we demonstrated that the average fiber distances and fiber densities were standard-

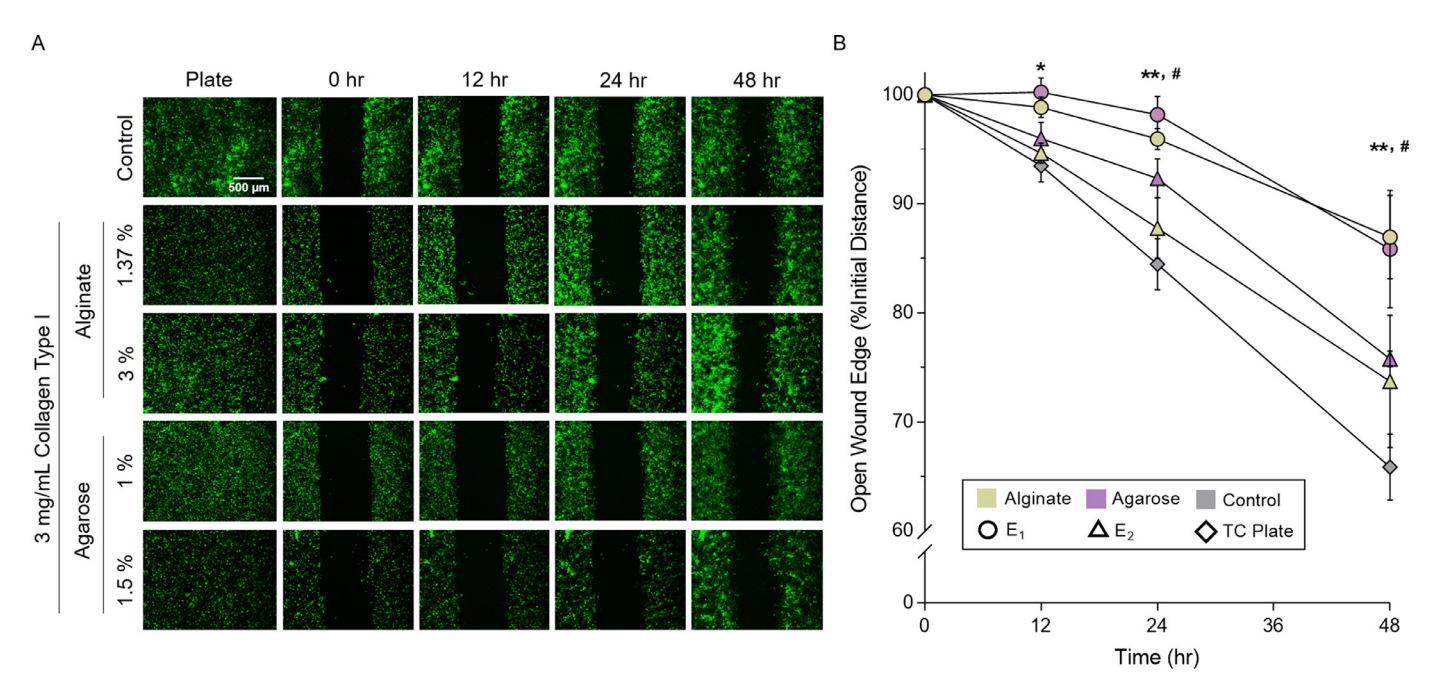


Fig. 5. Transduced stiffness utilizing IPN TME. **A.** Fluorescent images of recovered GFP⁺ OVCAR3, cultured in 1.37% alginate and 1% agarose IPNs plus 3 mg/mL collagen (low stiffness, E_1), 3% alginate and 1.5% agarose IPNs plus 3 mg/mL collagen (high stiffness, E_2), and tissue culture plate (2D controls) for 48 h. Cell migration was observed for an additional 48 h after a vertical wound was inflicted. **B.** Corresponding image-based quantification of cell migration (all data points were normalized to initial wound distance, $n \ge 3$ per condition). All data presented are means \pm SEMs; single and double asterisks (*, **) denote significance of P < 0.05 and 0.01 with regards to agarose IPNs respectively, while a hash-mark (#) denotes significance of P < 0.05 with regards to alginate IPNs, determined by ANOVA within each corresponding time point, followed by post-hoc analysis. (For interpretation of the references to colour in this figure legend, the reader is referred to the web version of this article.)

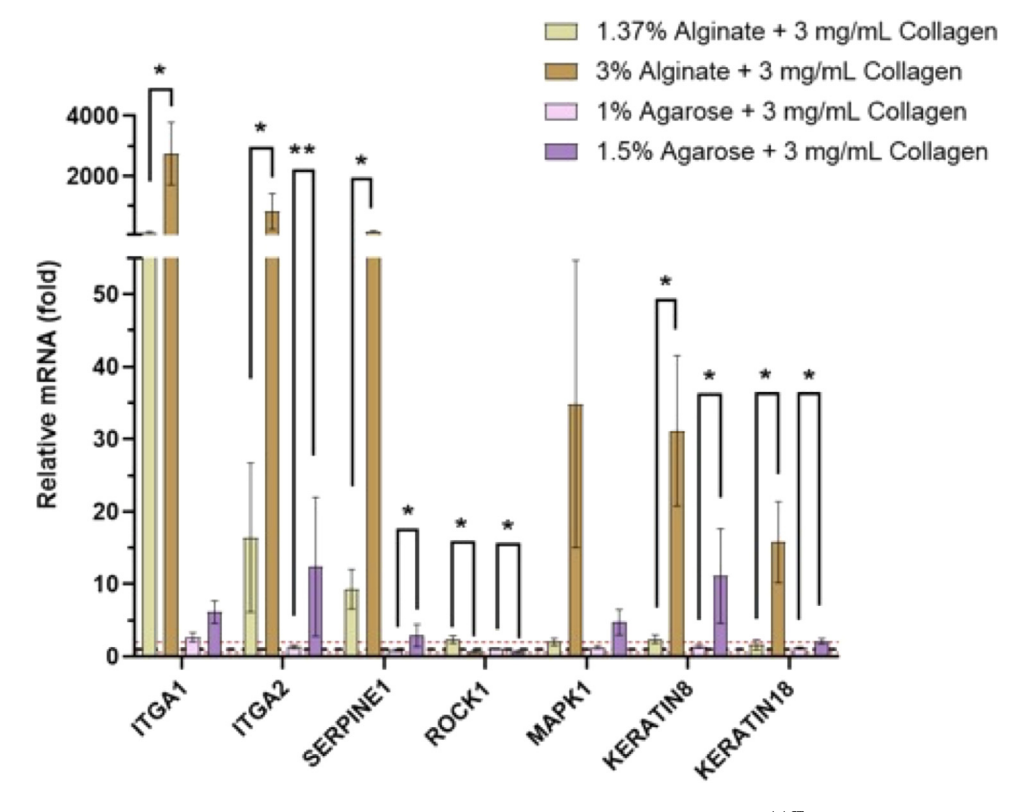


Fig. 6. Altered transcription in response to 3D IPN gels stiffness. Transcriptional assessment via quantitative PCR ($2^{\Delta\Delta CT}$, $n \ge 3$ per condition) for GFP⁺ OVCAR3, cultured in 1.37% alginate and 1% agarose IPNs plus 3 mg/mL collagen (low stiffness, E₁), 3% alginate and 1.5% agarose IPNs plus 3 mg/mL collagen (high stiffness, E₂), and tissue culture plate (2D controls) for 48 h. Trends display increased integrin, serpin, and MAPK related expression within the stiffer conditions. All data presented are means \pm SDs; single and double asterisks (*, **) denote significance of P < 0.05 and 0.01, determined by Mann-Whitney U test when comparing responses in IPNs. The dotted black line represents gene expression in the 2D condition. (For interpretation of the references to colour in this figure legend, the reader is referred to the web version of this article.)

ized to collagen content [101]. However, we observed variations in the average fiber distance between agarose and alginate semi-IPNs. These variations were attributed to disparities in thermodynamics at mixing, secondary or hydrogen bonding between polymers, and differing techniques used during polymerization. Further, agarose polymer structures undergo gelation quicker than alginate, which may account for differences observed in fiber formation and miscibility.

We further illustrated fiber dispersion in samples dehydrated via CPD. A pore size gradient is normally observed in relation to polysaccharide content [52,102], yet this trend was difficult to discern in the present study. To our knowledge this is the first time nanoarchitecture has been recorded at these precursor agarose and alginate concentrations. As expected, nanoarchitecture was more homogenous in hydrogels than in DPDXTs. The DPDXT samples displayed a wide variety of irregular ECM morphology, as previously described [18]. Although pore size was not replicated between in vitro IPNs and DPDXTs, the hydrogel homogeneity lends itself well to mechanobiology and the application of physical forces in vitro. We further investigated pore structure by observing similar permeability and porosity between 2% (w/v) agarose with 1 mg/mL collagen and DPDXTs. Alginate IPNs degraded significantly during HMDS sample preparation, making high-throughput dehydration via HMDS impracticable for alginate hydrogels. In future investigations, we propose measuring permeability and porosity with hydrogel samples prepared via CPD for direct comparison.

We determined that the precursor concentrations of agarose and alginate in each respective IPN hydrogel were the main determinant of shear storage modulus (G'). By varying agarose and alginate concentration, we adjusted the IPN stiffness to encompass the range found within ovarian tumors [40,41,53]. Yet limited by the viscosity of precursor alginate solutions, alginate-collagen IPNs were unable to match elastic moduli over 10.5 kPa [103]. To improve upon this range, higher calcium ion concentrations and alginate polymers with higher G to M block ratios can be used. Investigating these effects in the context of luer-lock mixed alginatecollagen IPNs is required to improve elastic moduli. Although both adhesion motif concentration and matrix stiffness impact tumor cell phenotype, many bioengineering models negate at least one of these two signals [33,55,67,68,101,104]. In contrast, the IPN hydrogels reported here can be used to combine these inputs without the added constraint of adverse coupling effects.

Investigating in vitro parameters further, we displayed excellent cellular viability and a remarkable capacity for in situ live-cell imaging in both IPN systems maintained over a period of 48 h. Most notably, we also demonstrated rigorous live-cell retrieval over this time period. Historically, separating live-cells from scaffolds is a difficult process and was theorized to be impossible for cells embedded in agarose [80-84,105,106]. Our approach was the first to utilize agarase enzyme, gentle mixing, and filtering techniques to recover cells with robust standard of viability. Although not required for the cell recovery above, we recommend including collagenase enzyme for studies involving concentrations of collagen above 3 mg/mL. Supplementing alginate culture medium with an external calcium source is also recommended in experiments surpassing 72 h, as this will mitigate the effects of ionic leaching. Separating cells from hydrogel vastly improves cell lysate quality, and by extension RNA and protein sequestration. We also validated the use of flow cytometry for measurement of cellular viability, and wound healing assays by sorting recovered cells for ethidium homodimer and GFP+expression, respectively. Cells cultured in IPNs of variable stiffness displayed a modest increase in migration with stiffer conditions, more closely resembling cells grown on tissue culture plates (E = 10,000 kPa). Importantly, differential expression of cell migratory behavior was observed after removal from 3D semi-IPN models. This moderate display of phenotypic memory implicates ECM stiffness in the process of EMT. Considering that this link is highly contested in previous ovarian cancer studies, further investigation is warranted [40,92,107-109]. The majority of studies relating to stiffness in ovarian cancers are conducted on 2D substrates and demonstrate signal transduction through the Rho/Rock or YAP/TAZ pathway [40,92-94]. However recent PDX tumor analysis may demonstrate that Rho/Rock and YAP/TAZ pathways are not activated in vivo, and instead involve the activation of MAPK/MEK in stiffer TME [25]. We identified trends that also support MAPK/MEK activation in response to increased ECM stiffness. Differences in gene expression between polysaccharide compartments may indicate a degree of implicit bioactive effect or an artifact from hydrogel degradation and warrants further investigation. Moreover, these experiments displayed the importance of replicating in vivo mechanical environments in 3D model systems, as biophysical stimuli impact cell behavior. Ultimately, agarose-collagen and alginate-collagen IPNs provide an exceptional matrix for the study of mechanobiology allowing for homogeneity in ultrastructure, fluid perfusion flow, and collagen spacing, as well as injection mold compatibility, excellent load transfer, and physiologically pertinent modulus.

5. Conclusion

The ovarian cancer TME is composed of an amalgam of extracellular components that interact dynamically to aid in the progression, metastases and chemoresistance of ovarian cancers. By omitting many of these factors, cellular cues and epigenetic changes are lost that may otherwise impact our understanding of ovarian tumorigenesis. For this reason, we present and characterize two comparable 3D semi-IPN hydrogel systems that accurately model the ECM found within ovarian tumors. Biochemical signaling, governed by collagen type I in tumors, can be manipulated in vitro to replicate fiber spacing pertinent to epithelial ovarian cancers. Utilizing straightforward alterations to precursor alginate and agarose concentrations, both nanoarchitecture and matrix stiffness can be finely tuned as required to create a unique and biologicallyreplicable TME. Both IPN hydrogels illustrate superior cell-viability in 3D encapsulation and growth, high-resolution live-cell imaging, and live-cell recovery. Together these findings support the utility of agarose-collagen and alginate-collagen semi-IPNs to study mechanobiology, as well as the roles of ECM in ovarian cancer progression.

Funding

This work is supported primarily by the American Cancer Society Research Scholar Award RSG-19-003-01-CCE (G.M.), the Office of the Assistant Secretary of Defense for Health Affairs through the Ovarian Cancer Research Program under Award No. W81XWH-16-1-0426 (G.M.), W81XWH-13-1-0134 (G.M.), DOD Investigator Initiated award W81XWH-18-0346 (G.M.), Rivkin Center for Ovarian Cancer (G.M.), and the Michigan Ovarian Cancer Alliance (G.M.), NSF EFRI DChem (Award number 2,029,139), NIH/NIDCR Tissue Engineering and Regeneration Training Grant T32DE00007057 (M. E. B.). Research reported in this publication was supported by the National Cancer Institute under award number P30CA046592 and by the National Institutes of Health under grant number UL1TR002240.

Data availability

The data that support the findings of this study are available from the corresponding author, upon reasonable request.

Declaration of Competing Interest

The authors declare that they have no known competing financial interests or personal relationships that could have appeared to influence the work reported in this paper.

Acknowledgments

We gratefully acknowledge the contributions of ovarian cancer advocates and patients for their support of cancer research and for donating tissues for portions of the work entailed here. We would like to thank Woo Jung Cho and Devon Leroux at the Microscopy and Image Analysis Laboratory (MIL) at University of Michigan's School of Medicine for assistance with electron microscopy sample preparation. We are grateful to Dr. S. Spanninga at the Biointerfaces Institute for technical assistance with mercury porosimetry, and the Michigan Center for Materials Characterization (MC2) for technical support. We would also like to acknowledge Hina Khan for assistance with researching collagen nucleation kinetics, as well as Huan Jiang and Nicole Wang for their work on alginate and agarose characterization. Finally, we are grateful to the high school level, undergraduate level and master's degree mentees, who have contributed to the different aspects of hydrogel polymerization and mechanobiology in our lab. The departments of Materials Science and Biomedical Engineering at the University of Michigan also deserve immense credit for fostering an inclusive environment for current and future scientists and researchers of all educational levels.

Supplementary materials

Supplementary material associated with this article can be found, in the online version, at doi:10.1016/j.actbio.2022.04.039.

References

- R.L. Siegel, K.D. Miller, H.E. Fuchs, A. Jemal, Cancer Statistics, 2021, CA Cancer J. Clin. 71 (2021) 7–33, doi:10.3322/caac.21654.
- [2] E. Lengyel, Ovarian Cancer Development and Metastasis, Am. J. Pathol. 177 (2010) 1053–1064, doi:10.2353/ajpath.2010.100105.
- [3] C.D. Vrabie, A. Petrescu, M. Waller, I. Dina, Clinical factors and biomarkers in ovarian tumors development, Rom. J. Morphol. Embryol. 49 (2008) 327–338.
- [4] T. Motohara, K. Masuda, M. Morotti, Y. Zheng, S. El-Sahhar, K.Y. Chong, N. Wietek, A. Alsaadi, M. Karaminejadranjbar, Z. Hu, M. Artibani, L.S. Gonzalez, H. Katabuchi, H. Saya, A.A. Ahmed, An evolving story of the metastatic voyage of ovarian cancer cells: cellular and molecular orchestration of the adipose-rich metastatic microenvironment, Oncogene 38 (2019) 2885–2898, doi:10.1038/s41388-018-0637-x.
- [5] K. Lawrenson, S.A. Gayther, Ovarian Cancer: a Clinical Challenge That Needs Some Basic Answers, PLoS Med. 6 (2009) e1000025, doi:10.1371/journal. pmed.1000025.
- [6] J.T. Thigpen, D. Alberts, M. Birrer, L. Copeland, R.L. Coleman, M. Markman, R.C. Bast, E.L. Eisenhauer, G. Fleming, P.M. Fracasso, D.M. Gershenson, T. Herzog, B.J. Monk, R.F. Ozols, G. Rustin, M.F. Brady, M. Shrader, A. Ranganathan, Current challenges and future directions in the management of ovarian cancer: proceedings of the first global workshop on ovarian cancer, Clin. Ovarian Cancer 3 (2010) 81–97, doi:10.3816/COC.2010.n.015.
- [7] U. Menon, A. Gentry-Maharaj, M. Burnell, N. Singh, A. Ryan, C. Karpinskyj, G. Carlino, J. Taylor, S.K. Massingham, M. Raikou, J.K. Kalsi, R. Woolas, R. Manchanda, R. Arora, L. Casey, A. Dawnay, S. Dobbs, S. Leeson, T. Mould, M.W. Seif, A. Sharma, K. Williamson, Y. Liu, L. Fallowfield, A.J. McGuire, S. Campbell, S.J. Skates, I.J. Jacobs, M. Parmar, Ovarian cancer population screening and mortality after long-term follow-up in the UK Collaborative Trial of Ovarian Cancer Screening (UKCTOCS): a randomised controlled trial, Lancet North Am. Ed. 397 (2021) 2182–2193, doi:10.1016/S0140-6736(21)00731-5.
- [8] D. Bell, A. Berchuck, M. Birrer, J. Chien, D.W. Cramer, F. Dao, R. Dhir, P. DiSaia, H. Gabra, P. Glenn, A.K. Godwin, J. Gross, L. Hartmann, M. Huang, D.G. Huntsman, M. Iacocca, M. Imielinski, S. Kalloger, B.Y. Karlan, D.A. Levine, G.B. Mills, C. Morrison, D. Mutch, N. Olvera, S. Orsulic, K. Park, N. Petrelli, B. Rabeno, J.S. Rader, B.I. Sikic, K. Smith-McCune, A.K. Sood, D. Bowtell, R. Penny, J.R. Testa, K. Chang, C.J. Creighton, H.H. Dinh, J.A. Drummond, G. Fowler, P. Gunaratne, A.C. Hawes, C.L. Kovar, L.R. Lewis, M.B. Morgan, I.F. Newsham, J. Santibanez, J.G. Reid, L.R. Trevino, Y.-Q. Wu, M. Wang, D.M. Muzny, D.A. Wheeler, R.A. Gibbs, G. Getz, M.S. Lawrence, K. Cibulskis, A.Y. Sivachenko, C. Sougnez, D. Voet, J. Wilkinson, T. Bloom, K. Ardlie, T. Fennell, J. Baldwin, R. Nichol,

S. Fisher, S. Gabriel, E.S. Lander, L. Ding, R.S. Fulton, D.C. Koboldt, M.D. McLellan, T. Wylie, J. Walker, M. O'Laughlin, D.J. Dooling, L. Fulton, R. Abbott, N.D. Dees, Q. Zhang, C. Kandoth, M. Wendl, W. Schierding, D. Shen, C.C. Harris, H. Schmidt, J. Kalicki, K.D. Delehaunty, C.C. Fronick, R. Demeter, L. Cook, J.W. Wallis, L. Lin, V.J. Magrini, J.S. Hodges, J.M. Eldred, S.M. Smith, C.S. Pohl, F. Vandin, E. Upfal, B.J. Raphael, G.M. Weinstock, E.R. Mardis, R.K. Wilson, M. Meyerson, W. Winckler, G. Getz, R.G.W. Verhaak, S.L. Carter, C.H. Mermel, G. Saksena, H. Nguyen, R.C. Onofrio, M.S. Lawrence, D. Hubbard, S. Gupta, A. Crenshaw, A.H. Ramos, K. Ardlie, L. Chin, A. Protopopov, J. Zhang, T.M. Kim, I. Perna, Y. Xiao, H. Zhang, G. Ren, N. Sathiamoorthy, R.W. Park, E. Lee, P.J. Park, R. Kucherlapati, D.M. Absher, L. Waite, G. Sherlock, J.D. Brooks, J.Z. Li, J. Xu, R.M. Myers, P.W. Laird, L. Cope, J.G. Herman, H. Shen, D.J. Weisenberger, H. Noushmehr, F. Pan, T. Triche Jr, B.P. Berman, D.J. Van Den Berg, J. Buckley, S.B. Baylin, P.T. Spellman, E. Purdom, P. Neuvial, H. Bengtsson, L.R. Jakkula, S. Durinck, J. Han, S. Dorton, H. Marr, Y.G. Choi, V. Wang, N.J. Wang, J. Ngai, J.G. Conboy, B. Parvin, H.S. Feiler, T.P. Speed, J.W. Gray, D.A. Levine, N.D. Socci, Y. Liang, B.S. Taylor, N. Schultz, L. Borsu, A.E. Lash, C. Brennan, A. Viale, C. Sander, M. Ladanyi, K.A. Hoadley, S. Meng, Y. Du, Y. Shi, L. Li, Y.J. Turman, D. Zang, E.B. Helms, S. Balu, X. Zhou, J. Wu, M.D. Topal, D.N. Hayes, C.M. Perou, G. Getz, D. Voet, G. Saksena, J. Zhang, H. Zhang, C.J. Wu, S. Shukla, K. Cibulskis, M.S. Lawrence, A. Sivachenko, R. Jing, R.W. Park, Y. Liu, P.J. Park, M. Noble, L. Chin, H. Carter, D. Kim, J. Samayoa, R. Karchin, P.T. Spellman, E. Purdom, P. Neuvial, H. Bengtsson, S. Durinck, J. Han, J.E. Korkola, L.M. Heiser, R.J. Cho, Z. Hu, B. Parvin, T.P. Speed, J.W. Gray, N. Schultz, E. Cerami, B.S. Taylor, A. Olshen, B. Reva, Y. Antipin, R. Shen, P. Mankoo, R. Sheridan, G. Ciriello, W.K. Chang, J.A. Bernanke, L. Borsu, D.A. Levine, M. Ladanyi, C. Sander, D. Haussler, C.C. Benz, J.M. Stuart, S.C. Benz, J.Z. Sanborn, C.J. Vaske, J. Zhu, C. Szeto, G.K. Scott, C. Yau, K.A. Hoadley, Y. Du, S. Balu, D.N. Hayes, C.M. Perou, M.D. Wilkerson, N. Zhang, R. Akbani, K.A. Baggerly, W.K. Yung, G.B. Mills, J.N. Weinstein, R. Penny, T. Shelton, D. Grimm, M. Hatfield, S. Morris, P. Yena, P. Rhodes, M. Sherman, J. Paulauskis, S. Millis, A. Kahn, J.M. Greene, The Cancer Genome Atlas Research Network, (Participants are arranged by area of contribution and then by institution.), Disease working group and tissue source sites, Genome sequencing centres: baylor College of Medicine, Broad Institute, Washington University in St Louis, Cancer genome characterization centres: broad Institute/Dana-Farber Cancer Institute, Harvard Medical School, HudsonAlpha Institute/Stanford University, University of Southern California/Johns Hopkins University, Lawrence Berkeley National Laboratory, Memorial Sloan-Kettering Cancer Center, University of North Carolina at Chapel Hill, Genome data analysis centres: broad Institute, Johns Hopkins University, University of California Santa Cruz/Buck Institute, The University of Texas MD Anderson Cancer Center, Biospecimen core resource, Data coordination centre, Integrated genomic analyses of ovarian carcinoma, Nature. 474 (2011) 609-615, doi:10.1038/nature10166.

- [9] R.G.W. Verhaak, P. Tamayo, J.-Y. Yang, D. Hubbard, H. Zhang, C.J. Creighton, S. Fereday, M. Lawrence, S.L. Carter, C.H. Mermel, A.D. Kostic, D. Etemadmoghadam, G. Saksena, K. Cibulskis, S. Duraisamy, K. Levanon, C. Sougnez, A. Tsherniak, S. Gomez, R. Onofrio, S. Gabriel, L. Chin, N. Zhang, P.T. Spellman, Y. Zhang, R. Akbani, K.A. Hoadley, A. Kahn, M. Köbel, D. Huntsman, R.A. Soslow, A. Defazio, M.J. Birrer, J.W. Gray, J.N. Weinstein, D.D. Bowtell, R. Drapkin, J.P. Mesirov, G. Getz, D.A. Levine, M. Meyerson, Prognostically relevant gene signatures of high-grade serous ovarian carcinoma, J. Clin. Invest. 123 (2013) 517–525, doi:10.1172/[Cl65833.
- [10] R.W. Tothill, A.V. Tinker, J. George, R. Brown, S.B. Fox, S. Lade, D.S. Johnson, M.K. Trivett, D. Etemadmoghadam, B. Locandro, N. Traficante, S. Fereday, J.A. Hung, Y.-E. Chiew, I. Haviv, A.O.C.S. Group, D. Gertig, A. deFazio, D.D.L. Bowtell, Novel Molecular Subtypes of Serous and Endometrioid Ovarian Cancer Linked to Clinical Outcome, Clin. Cancer Res. 14 (2008) 5198–5208, doi:10.1158/1078-0432.CCR-08-0196.
- [11] H.S. Leong, L. Galletta, D. Etemadmoghadam, J. George, M. Köbel, S.J. Ramus, D. Bowtell, Efficient molecular subtype classification of high-grade serous ovarian cancer, J. Pathol. 236 (2015) 272–277, doi:10.1002/path.4536.
- [12] B. Izar, I. Tirosh, E.H. Stover, I. Wakiro, M.S. Cuoco, I. Alter, C. Rodman, R. Leeson, M.-J. Su, P. Shah, M. Iwanicki, S.R. Walker, A. Kanodia, J.C. Melms, S. Mei, J.-R. Lin, C.B.M. Porter, M. Slyper, J. Waldman, L. Jerby-Arnon, O. Ashenberg, T.J. Brinker, C. Mills, M. Rogava, S. Vigneau, P.K. Sorger, L.A. Garraway, P.A. Konstantinopoulos, J.F. Liu, U. Matulonis, B.E. Johnson, O. Rozenblatt-Rosen, A. Rotem, A. Regev, A single-cell landscape of high-grade serous ovarian cancer, Nat. Med. 26 (2020) 1271–1279, doi:10.1038/s41591-020-0926-0.
- [13] F. Chen, D.S. Chandrashekar, S. Varambally, C.J. Creighton, Pan-cancer molecular subtypes revealed by mass-spectrometry-based proteomic characterization of more than 500 human cancers, Nat. Commun. 10 (2019) 5679, doi:10.1038/s41467-019-13528-0.
- [14] M.E. Bregenzer, E.N. Horst, P. Mehta, C.M. Novak, T. Repetto, G. Mehta, The Role of Cancer Stem Cells and Mechanical Forces in Ovarian Cancer Metastasis, Cancers (Basel) (2019).
- [15] C. Novak, E. Horst, G. Mehta, Review: mechanotransduction in ovarian cancer: shearing into the unknown, APL Bioengineering 2 (2018) 031701, doi:10.1063/ 1.5024386.
- [16] D.C. Hinshaw, L.A. Shevde, The tumor microenvironment innately modulates cancer progression, Cancer Res. 79 (2019) 4557–4566, doi:10.1158/0008-5472. CAN-18-3962.
- [17] J.A. Eble, S. Niland, The extracellular matrix in tumor progression and metastasis, Clin. Exp. Metastasis 36 (2019) 171–198, doi:10.1007/ s10585-019-09966-1.

- [18] E.N. Horst, M.E. Bregenzer, P. Mehta, C.S. Snyder, T. Repetto, Y. Yang-Hartwich, G. Mehta, Personalized models of heterogeneous 3D epithelial tumor microenvironments: ovarian cancer as a model☆, Acta Biomater. (2021), doi:10. 1016/j.actbio.2021.04.041.
- [19] K. Dzobo, D.A. Senthebane, N.E. Thomford, A. Rowe, C. Dandara, M.I. Parker, Not Everyone Fits the Mold: intratumor and Intertumor Heterogeneity and Innovative Cancer Drug Design and Development, OMICS: J. Integr. Biol. 22 (2018) 17–34, doi:10.1089/omi.2017.0174.
- [20] M.J. Paszek, V.M. Weaver, The tension mounts: mechanics meets morphogenesis and malignancy, J. Mammary Gland Biol. Neoplasia 9 (2004) 325–342, doi:10.1007/s10911-004-1404-x.
- [21] Y. Zhao, J. Cao, A. Melamed, M. Worley, A. Gockley, D. Jones, H.T. Nia, Y. Zhang, T. Stylianopoulos, A.S. Kumar, F. Mpekris, M. Datta, Y. Sun, L. Wu, X. Gao, O. Yeku, M.G. Del Carmen, D.R. Spriggs, R.K. Jain, L. Xu, Losartan treatment enhances chemotherapy efficacy and reduces ascites in ovarian cancer models by normalizing the tumor stroma, Proc. Natl. Acad. Sci. U S A. 116 (2019) 2210–2219, doi:10.1073/pnas.1818357116.
- [22] B. Izar, I. Tirosh, E.H. Stover, I. Wakiro, M.S. Cuoco, I. Alter, C. Rodman, R. Leeson, M.-J. Su, P. Shah, M. Iwanicki, S.R. Walker, A. Kanodia, J.C. Melms, S. Mei, J.-R. Lin, C.B.M. Porter, M. Slyper, J. Waldman, L. Jerby-Arnon, O. Ashenberg, T.J. Brinker, C. Mills, M. Rogava, S. Vigneau, P.K. Sorger, L.A. Garraway, P.A. Konstantinopoulos, J.F. Liu, U. Matulonis, B.E. Johnson, O. Rozenblatt-Rosen, A. Rotem, A. Regev, A single-cell landscape of high-grade serous ovarian cancer, Nat. Med. 26 (2020) 1271–1279, doi:10.1038/s41591-020-0926-0.
- [23] F. Chen, D.S. Chandrashekar, S. Varambally, C.J. Creighton, Pan-cancer molecular subtypes revealed by mass-spectrometry-based proteomic characterization of more than 500 human cancers, Nat. Commun. 10 (2019) 5679, doi:10.1038/s41467-019-13528-0.
- [24] S. Kauppila, M.K. Bode, F. Stenbäck, L. Risteli, J. Risteli, Cross-linked telopeptides of type I and III collagens in malignant ovarian tumours in vivo, Br. J. Cancer 81 (1999) 654–661, doi:10.1038/sj.bjc.6690743.
- [25] V. Mieulet, C. Garnier, Y. Kieffer, T. Guilbert, F. Nemati, E. Marangoni, G. Renault, F. Chamming's, A. Vincent-Salomon, F. Mechta-Grigoriou, Stiffness increases with myofibroblast content and collagen density in mesenchymal high grade serous ovarian cancer, Sci. Rep. 11 (2021) 4219, doi:10.1038/s41598-021-83685-0.
- [26] C. Lan, A. Heindl, X. Huang, S. Xi, S. Banerjee, J. Liu, Y. Yuan, Quantitative histology analysis of the ovarian tumour microenvironment, Sci. Rep. 5 (2015) 16317, doi:10.1038/srep16317.
- [27] M.E. Bregenzer, E.N. Horst, P. Mehta, C.M. Novak, T. Repetto, G. Mehta, The Role of Cancer Stem Cells and Mechanical Forces in Ovarian Cancer Metastasis, Cancers (Basel) 11 (2019) 1008, doi:10.3390/cancers11071008.
- [28] P.A. Netti, D.A. Berk, M.A. Swartz, A.J. Grodzinsky, R.K. Jain, Role of extracellular matrix assembly in interstitial transport in solid tumors, Cancer Res. 60 (2000) 2497–2503.
- [29] M.H. Joyce, C. Lu, E.R. James, R. Hegab, S.C. Allen, L.J. Suggs, A. Brock, Phenotypic basis for matrix stiffness-dependent chemoresistance of breast cancer cells to doxorubicin, Front. Oncol. 8 (2018) 337, doi:10.3389/fonc.2018.00337.
- [30] A.-K. Lind, B. Weijdegård, P. Dahm-Kähler, J. Mölne, K. Sundfeldt, M. Brännström, Collagens in the human ovary and their changes in the perifollicular stroma during ovulation, Acta Obstet. Gynecol. Scand. 85 (2006) 1476–1484, doi:10.1080/00016340601033741.
- [31] C. Ricciardelli, R.J. Rodgers, Extracellular Matrix of Ovarian Tumors, Semin. Reprod. Med. 24 (2006) 270–282, doi:10.1055/s-2006-948556.
- [32] O.M.T. Pearce, R.M. Delaine-Smith, E. Maniati, S. Nichols, J. Wang, S. Böhm, V. Rajeeve, D. Ullah, P. Chakravarty, R.R. Jones, A. Montfort, T. Dowe, J. Gribben, J.L. Jones, H.M. Kocher, J.S. Serody, B.G. Vincent, J. Connelly, J.D. Brenton, C. Chelala, P.R. Cutillas, M. Lockley, C. Bessant, M.M. Knight, F.R. Balkwill, Deconstruction of a metastatic tumor microenvironment reveals a common matrix response in human cancers, Cancer Discov. 8 (2018) 304–319, doi:10.1158/2159-8290.CD-17-0284.
- [33] S. Alkmin, R. Brodziski, H. Simon, D. Hinton, R.H. Goldsmith, M. Patankar, P.J. Campagnola, Role of collagen fiber morphology on ovarian cancer cell migration using image-based models of the extracellular matrix, Cancers (Basel) 12 (2020) 1390, doi:10.3390/cancers12061390.
- [34] O. Nadiarnykh, R.B. LaComb, M.A. Brewer, P.J. Campagnola, Alterations of the extracellular matrix in ovarian cancer studied by Second Harmonic Generation imaging microscopy, BMC Cancer 10 (2010) 94, doi:10.1186/ 1421-2407-10.94
- [35] A. Naba, O.M.T. Pearce, A. Del Rosario, D. Ma, H. Ding, V. Rajeeve, P.R. Cutillas, F.R. Balkwill, R.O. Hynes, Characterization of the extracellular matrix of normal and diseased tissues using proteomics, J. Proteome Res. 16 (2017) 3083-3091, doi:10.1021/acs.jproteome.7b00191.
- [36] I. Acerbi, L. Cassereau, I. Dean, Q. Shi, A. Au, C. Park, Y.Y. Chen, J. Liphardt, E.S. Hwang, V.M. Weaver, Human breast cancer invasion and aggression correlates with ECM stiffening and immune cell infiltration, Integr. Biol. 7 (2015) 1120–1134, doi:10.1039/CSIB00040H.
- [37] P. Lu, V.M. Weaver, Z. Werb, The extracellular matrix: a dynamic niche in cancer progression, J. Cell Biol. 196 (2012) 395–406, doi:10.1083/jcb.201102147.
- [38] O. Maller, A.P. Drain, A.S. Barrett, S. Borgquist, B. Ruffell, I. Zakharevich, T.T. Pham, T. Gruosso, H. Kuasne, J.N. Lakins, I. Acerbi, J.M. Barnes, T. Nemkov, A. Chauhan, J. Gruenberg, A. Nasir, O. Bjarnadottir, Z. Werb, P. Kabos, Y.-Y. Chen, E.S. Hwang, M. Park, L.M. Coussens, A.C. Nelson, K.C. Hansen, V.M. Weaver, Tumour-associated macrophages drive stromal cell-dependent collagen crosslinking and stiffening to promote breast cancer aggression, Nat. Mater. (2020) 1–12, doi:10.1038/s41563-020-00849-5.

- [39] M.W. Pickup, H. Laklai, I. Acerbi, P. Owens, A.E. Gorska, A. Chytil, M. Aakre, V.M. Weaver, H.L. Moses, Stromally derived lysyl oxidase promotes metastasis of transforming growth factor-β-deficient mouse mammary carcinomas, Cancer Res. 73 (2013) 5336–5346, doi:10.1158/0008-5472.CAN-13-0012.
- [40] A.J. McKenzie, S.R. Hicks, K.V. Svec, H. Naughton, Z.L. Edmunds, A.K. Howe, The mechanical microenvironment regulates ovarian cancer cell morphology, migration, and spheroid disaggregation, Sci. Rep. 8 (2018) 7228, doi:10.1038/ s41598-018-25589-0.
- [41] A. Ansardamavandi, M. Tafazzoli-Shadpour, R. Omidvar, F. Nili, An AFM-based nanomechanical study of ovarian tissues with pathological conditions, Int. J. Nanomed. 15 (2020) 4333–4350, doi:10.2147/IJN.S254342.
- [42] E.S. Dragan, Advances in interpenetrating polymer network hydrogels and their applications, Pure Appl. Chem. 86 (2014) 1707–1721, doi:10.1515/ pac-2014-0713.
- [43] A.P. Dhand, J.H. Galarraga, J.A. Burdick, Enhancing biopolymer hydrogel functionality through interpenetrating networks, Trends Biotechnol. (2020) 0, doi:10.1016/j.tibtech.2020.08.007.
- [44] B.J. DeKosky, N.H. Dormer, G.C. Ingavle, C.H. Roatch, J. Lomakin, M.S. Detamore, S.H. Gehrke, Hierarchically designed agarose and poly(ethylene glycol) interpenetrating network hydrogels for cartilage tissue engineering, Tissue Eng. Part C Methods 16 (2010) 1533–1542, doi:10.1089/ten.tec.2009.0761.
- [45] S. Suri, C.E. Schmidt, Photopatterned collagen-hyaluronic acid interpenetrating polymer network hydrogels, Acta Biomater. 5 (2009) 2385–2397, doi:10. 1016/j.actbio.2009.05.004.
- [46] C.M. Novak, E.N. Horst, C.C. Taylor, C.Z. Liu, G. Mehta, Fluid shear stress stimulates breast cancer cells to display invasive and chemoresistant phenotypes while upregulating PLAU in a 3D bioreactor, Biotechnol. Bioeng. 116 (2019) 3084–3097, doi:10.1002/bit.27119.
- [47] C.M. Novak, E.N. Horst, E. Lin, G. Mehta, Compressive stimulation enhances ovarian cancer proliferation, invasion, chemoresistance, and mechanotransduction via CDC42 in a 3D bioreactor, Cancers (Basel) 12 (2020) 1521, doi:10. 3390/cancers12061521.
- [48] P.K. Walsh, F.V. Isdell, S.M. Noone, M.G. O'Donovan, D.M. Malone, Growth patterns of Saccharomyces cerevisiae microcolonies in alginate and carrageenan gel particles: effect of physical and chemical properties of gels, Enzyme and Microbial Technology. 18 (1996) 366–372. https://doi.org/10.1016/0141-0229/95)00135-2.
- [49] T.S. Pathak, J.-.H. Yun, J. Lee, K.-.J. Paeng, Effect of calcium ion (cross-linker) concentration on porosity, surface morphology and thermal behavior of calcium alginates prepared from algae (Undaria pinnatifida), Carbohydrate Polym. 81 (2010) 633–639, doi:10.1016/j.carbpol.2010.03.025.
- [50] A.J. Fleszar, A. Walker, P.K. Kreeger, J. Notbohm, Substrate curvature induces fallopian tube epithelial cell invasion via cell-cell tension in a model of ovarian cortical inclusion cysts, Int. Bio (Cam) 11 (2019) 342–352, doi:10.1093/ intbio/zyz028.
- [51] T.A. Ulrich, T.G. Lee, H.K. Shon, D.W. Moon, S. Kumar, Microscale mechanisms of agarose-induced disruption of collagen remodeling, Biomaterials 32 (2011) 5633–5642, doi:10.1016/j.biomaterials.2011.04.045.
- [52] T.A. Ulrich, A. Jain, K. Tanner, J.L. MacKay, S. Kumar, Probing cellular mechanobiology in three-dimensional culture with collagen-agarose matrices, Biomaterials 31 (2010) 1875–1884, doi:10.1016/j.biomaterials.2009.10.047.
- [53] C.T. Buckley, S.D. Thorpe, F.J. O'Brien, A.J. Robinson, D.J. Kelly, The effect of concentration, thermal history and cell seeding density on the initial mechanical properties of agarose hydrogels, J. Mech. Behav. Biomed. Mater. 2 (2009) 512–521, doi:10.1016/j.jmbbm.2008.12.007.
- [54] S.M. O'Connor, D.A. Stenger, K.M. Shaffer, W. Ma, Survival and neurite out-growth of rat cortical neurons in three-dimensional agarose and collagen gel matrices, Neurosci. Lett. 304 (2001) 189–193, doi:10.1016/S0304-3940(01) 01769-4.
- [55] G. Xu, F. Yin, H. Wu, X. Hu, L. Zheng, J. Zhao, In vitro ovarian cancer model based on three-dimensional agarose hydrogel, J. Tissue Eng. 5 (2014), doi:10. 1177/2041731413520438.
- [56] B.M. Gillette, J.A. Jensen, B. Tang, G.J. Yang, A. Bazargan-Lari, M. Zhong, S.K. Sia, In situ collagen assembly for integrating microfabricated threedimensional cell-seeded matrices, Nat. Mater. 7 (2008) 636–640, doi:10.1038/ nmat2203.
- [57] S. Shin, M. Ikram, F. Subhan, H. Yeong Kang, Y. Lim, R. Lee, S. Jin, Y. Hun Jeong, J.--Y. Kwak, Y.--J. Na, S. Yoon, Alginate-marine collagen-agarose composite hydrogels as matrices for biomimetic 3D cell spheroid formation, RSC Adv. 6 (2016) 46952–46965, doi:10.1039/C6RA01937D.
- [58] T. de Chalain, J.H. Phillips, A. Hinek, Bioengineering of elastic cartilage with aggregated porcine and human auricular chondrocytes and hydrogels containing alginate, collagen, and kappa-elastin, J. Biomed. Mater. Res. 44 (1999) 280–288, doi:10.1002/(sici)1097-4636(19990305)44:3(280::aid-jbm6) 3.0.co;2-h.
- [59] S. Loty, N. Forest, H. Boulekbache, J.-.M. Sautier, Cytochalasin D induces changes in cell shape and promotes in vitro chondrogenesis: a morphological study, Biol. Cell 83 (1995) 149–161, doi:10.1016/0248-4900(96)81303-7.
- [60] M.R. Ward Rashidi, P. Mehta, M. Bregenzer, S. Raghavan, E.M. Fleck, E.N. Horst, Z. Harissa, V. Ravikumar, S. Brady, A. Bild, A. Rao, R.J. Buckanovich, G. Mehta, Engineered 3D model of cancer stem cell enrichment and chemoresistance, Neoplasia 21 (2019) 822–836, doi:10.1016/j.neo.2019.06.005.
- [61] M.E. Bregenzer, C. Davis, E.N. Horst, P. Mehta, C.M. Novak, S. Raghavan, C.S. Snyder, G. Mehta, Physiologic patient derived 3D spheroids for anti-neoplastic drug screening to target cancer stem cells, JoVE (J. Visualized Exper.) (2019) e59696, doi:10.3791/59696.

- [62] S. Raghavan, P. Mehta, E.N. Horst, M.R. Ward, K.R. Rowley, G. Mehta, Comparative analysis of tumor spheroid generation techniques for differential in vitro drug toxicity, Oncotarget 7 (2016) 16948–16961, doi:10.18632/oncotarget. 7659
- [63] V. Normand, D.L. Lootens, E. Amici, K.P. Plucknett, P. Aymard, New insight into agarose gel mechanical properties, Biomacromolecules 1 (2000) 730–738, doi:10.1021/bm005583i.
- [64] R. Camba, Mechanical properties of hydrated acoustically sensitive alginate-based microcapsules confined in a microfluidic device as a function of size and composition, J Biotechnol. Biomater. (2013) 03, doi:10.4172/2155-952X. 1000161.
- [65] M. Ahearne, Y. Yang, A.J. El Haj, K.Y. Then, K.-.K. Liu, Characterizing the viscoelastic properties of thin hydrogel-based constructs for tissue engineering applications, J. R. Soc. Interface 2 (2005) 455–463, doi:10.1098/rsif.2005.0065.
- [66] G. Rijal, W. Li, A versatile 3D tissue matrix scaffold system for tumor modeling and drug screening, Sci. Adv. 3 (2017) e1700764, doi:10.1126/sciadv. 1700764.
- [67] M. Liu, X. Zhang, C. Long, H. Xu, X. Cheng, J. Chang, C. Zhang, C. Zhang, X. Wang, Collagen-based three-dimensional culture microenvironment promotes epithelial to mesenchymal transition and drug resistance of human ovarian cancer in vitro, RSC Adv. 8 (2018) 8910–8919, doi:10.1039/C7R413742G.
- [68] A.J. Fleszar, A. Walker, V. Porubsky, W. Flanigan, D. James, P.J. Campagnola, P.S. Weisman, P.K. Kreeger, The extracellular matrix of ovarian cortical inclusion cysts modulates invasion of fallopian tube epithelial cells, APL Bioeng. 2 (2018), doi:10.1063/1.5022595.
- [69] C.B. Raub, V. Suresh, T. Krasieva, J. Lyubovitsky, J.D. Mih, A.J. Putnam, B.J. Tromberg, S.C. George, Noninvasive assessment of collagen gel microstructure and mechanics using multiphoton microscopy, Biophys. J. 92 (2007) 2212–2222, doi:10.1529/biophysj.106.097998.
- [70] A.D. Doyle, Generation of 3D collagen gels with controlled, diverse architectures, Curr. Protoc. Cell Biol. 72 (2016) 10.20.1-10.20.16, doi:10.1002/cpcb.9.
- [71] J. Rosenblatt, B. Devereux, D.G. Wallace, Injectable collagen as a pH-sensitive hydrogel, Biomaterials 15 (1994) 985–995, doi:10.1016/0142-9612(94) 90079-5.
- [72] G.P. Dillon, X. Yu, A. Sridharan, J.P. Ranieri, R.V. Bellamkonda, The influence of physical structure and charge on neurite extension in a 3D hydrogel scaffold, J. Biomater. Sci. Polym. Ed. 9 (1998) 1049–1069, doi:10.1163/156856298x00325.
- [73] A. Pluen, P.A. Netti, R.K. Jain, D.A. Berk, Diffusion of macromolecules in agarose gels: comparison of linear and globular configurations, Biophys. J. 77 (1999) 542–552, doi:10.1016/S0006-3495(99)76911-0.
- [74] K.B. Kosto, W.M. Deen, Diffusivities of macromolecules in composite hydrogels, AlChE J. 50 (2004) 2648–2658, doi:10.1002/aic.10216.
- [75] M. Baniasadi, M. Minary-Jolandan, Alginate-collagen fibril composite hydrogel, Materials (Basel) 8 (2015) 799–814, doi:10.3390/ma8020799.
- [76] F. Tanaka, M. Ishida, Thermoreversible gelation with two-component networks, Macromolecules 32 (1999) 1271–1283, doi:10.1021/ma981279v.
- [77] X. Zhao, A theory for large deformation and damage of interpenetrating polymer networks, J. Mech. Phys. Solids 60 (2012) 319–332, doi:10.1016/j.jmps. 2011.10.005.
- [78] G. Scionti, M. Moral, M. Toledano, R. Osorio, J.D.G. Durán, M. Alaminos, A. Campos, M.T. López-López, Effect of the hydration on the biomechanical properties in a fibrin-agarose tissue-like model, J. Biomed. Mater. Res. A 102 (2014) 2573–2582, doi:10.1002/jbm.a.34929.
- [79] P. Duan, N. Kandemir, J. Wang, J. Chen, Rheological characterization of alginate based hydrogels for tissue engineering, MRS Adv. 2 (2017) 1309–1314, doi:10.1557/adv.2017.8.
- [80] C. Mulas, A.C. Hodgson, T.N. Kohler, C.C. Agley, F. Hollfelder, A. Smith, K. Chalut, Microfluidic platform for live cell imaging of 3D cultures with clone retrieval, bioRxiv (2020) 2020.02.17.952689, doi:10.1101/2020.02.17.952689.
- [81] M. Schindler, D. Siriwardena, T.N. Kohler, A.L. Ellermann, E. Slatery, C. Munger, F. Hollfelder, T.E. Boroviak, Agarose microgel culture delineates lumenogenesis in naive and primed human pluripotent stem cells, Stem Cell Rep. 16 (2021) 1347–1362, doi:10.1016/j.stemcr.2021.04.009.
- [82] E. Afrimzon, G. Botchkina, N. Zurgil, Y. Shafran, M. Sobolev, S. Moshkov, O. Ravid-Hermesh, I. Ojima, M. Deutsch, Hydrogel microstructure live-cell array for multiplexed analyses of cancer stem cells, tumor heterogeneity and differential drug response at single-element resolution, Lab Chip 16 (2016) 1047-1062, doi:10.1039/C6LC00014B.
- [83] F. Akther, P. Little, Z. Li, N.-.T. Nguyen, H.T. Ta, Hydrogels as artificial matrices for cell seeding in microfluidic devices, RSC Adv. 10 (2020) 43682–43703, doi:10.1039/D0RA08566A.
- [84] M.A. Salati, J. Khazai, A.M. Tahmuri, A. Samadi, A. Taghizadeh, M. Taghizadeh, P. Zarrintaj, J.D. Ramsey, S. Habibzadeh, F. Seidi, M.R. Saeb, M. Mozafari, Agarose-based biomaterials: opportunities and challenges in cartilage tissue engineering, Polymers (Basel) 12 (2020) 1150, doi:10.3390/polym12051150.
- [85] J. Heino, The collagen family members as cell adhesion proteins, Bioessays 29 (2007) 1001–1010, doi:10.1002/bies.20636.
- [86] S. Nasrollahi, C. Walter, A.J. Loza, G.V. Schimizzi, G.D. Longmore, A. Pathak, Past matrix stiffness primes epithelial cells and regulates their future collective migration through a mechanical memory, Biomaterials 146 (2017) 146– 155, doi:10.1016/j.biomaterials.2017.09.012.

- [87] C. Yang, M.W. Tibbitt, L. Basta, K.S. Anseth, Mechanical memory and dosing influence stem cell fate, Nature Mater. 13 (2014) 645–652, doi:10.1038/nmaf3889.
- [88] I. Carnevale, M. Capula, E. Giovannetti, T. Schmidt, S. Coppola, A mechanical memory of pancreatic cancer cells, 2019. https://doi.org/10.1101/730960.
- [89] A.W. Watson, A.D. Grant, S.S. Parker, S. Hill, M.B. Whalen, J. Chakrabarti, M.W. Harman, M.R. Roman, B.L. Forte, C.C. Gowan, R. Castro-Portuguez, L.K. Stolze, C. Franck, D.A. Cusanovich, Y. Zavros, M. Padi, C.E. Romanoski, G. Mouneimne, Breast tumor stiffness instructs bone metastasis via maintenance of mechanical conditioning, Cell Rep. 35 (2021) 109293, doi:10.1016/j.celrep.2021.109293.
- [90] C.X. Li, N.P. Talele, S. Boo, A. Koehler, E. Knee-Walden, J.L. Balestrini, P. Speight, A. Kapus, B. Hinz, MicroRNA-21 preserves the fibrotic mechanical memory of mesenchymal stem cells, Nature Mater. 16 (2017) 379–389, doi:10.1038/nmat4780.
- [91] J.L. Balestrini, S. Chaudhry, V. Sarrazy, A. Koehler, B. Hinz, The mechanical memory of lung myofibroblasts, Integr. Biol. 4 (2012) 410–421, doi:10.1039/ c2ib00149g.
- [92] D.J. McGrail, Q.M.N. Kieu, M.R. Dawson, The malignancy of metastatic ovarian cancer cells is increased on soft matrices through a mechanosensitive Rho-ROCK pathway, J. Cell Sci. 127 (2014) 2621–2626, doi:10.1242/jcs.144378.
- [93] X. Wei, H. Lou, D. Zhou, Y. Jia, H. Li, Q. Huang, J. Ma, Z. Yang, C. Sun, Y. Meng, S. Xu, X. Yang, X. Li, T. Ji, Z. Guo, Q. Gao, TAGLN mediated stiffness-regulated ovarian cancer progression via RhoA/ROCK pathway, J. Exp. Clin. Cancer Res. 40 (2021) 292, doi:10.1186/s13046-021-02091-6.
- [94] Y. Fan, Q. Sun, X. Li, J. Feng, Z. Ao, X. Li, J. Wang, Substrate stiffness modulates the growth, phenotype, and chemoresistance of ovarian cancer cells, Front. Cell Dev. Biol. 9 (2021) 2263, doi:10.3389/fcell.2021.718834.
- [95] M.E. Bregenzer, E.N. Horst, P. Mehta, C.M. Novak, S. Raghavan, C.S. Snyder, G. Mehta, Integrated cancer tissue engineering models for precision medicine, PLoS One 14 (2019) e0216564, doi:10.1371/journal.pone.0216564.
- [96] H. Geckil, F. Xu, X. Zhang, S. Moon, U. Demirci, Engineering hydrogels as extracellular matrix mimics, Nanomedicine 5 (2010) 469–484, doi:10.2217/nnm. 10.12.
- [97] Y. Ling, J. Rubin, Y. Deng, C. Huang, U. Demirci, J.M. Karp, A. Khademhosseini, A cell-laden microfluidic hydrogel, Lab Chip 7 (2007) 756–762, doi:10.1039/ B615486G.
- [98] A. Cho, V.M. Howell, E.K. Colvin, The extracellular matrix in epithelial ovarian cancer – a piece of a puzzle, Front. Oncol. 5 (2015), doi:10.3389/fonc.2015. 00245.
- [99] E. Flate, J.R.D. Stalvey, Motility of select ovarian cancer cell lines: effect of extra-cellular matrix proteins and the involvement of PAK2, Int. J. Oncol. 45 (2014) 1401–1411, doi:10.3892/ijo.2014.2553.
- [100] N. Ahmed, K.L. Stenvers, Getting to know ovarian cancer ascites: opportunities for targeted therapy-based translational research, Front. Oncol. 3 (2013), doi:10.3389/fonc.2013.00256.
- [101] A.J. Berger, K.M. Linsmeier, P.K. Kreeger, K.S. Masters, Decoupling the effects of stiffness and fiber density on cellular behaviors via an interpenetrating network of gelatin-methacrylate and collagen, Biomaterials 141 (2017) 125– 135, doi:10.1016/j.biomaterials.2017.06.039.
- [102] C. Ort, Y. Chen, A. Ghagre, A. Ehrlicher, C. Moraes, Bioprintable, stiffness-tunable collagen-alginate microgels for increased throughput 3D cell culture studies, ACS Biomater. Sci. Eng. (2021), doi:10.1021/acsbiomaterials.1c00129.
- [103] C. Branco da Cunha, D.D. Klumpers, W.A. Li, S.T. Koshy, J.C. Weaver, O. Chaudhuri, P.L. Granja, D.J. Mooney, Influence of the stiffness of three-dimensional alginate/collagen-I interpenetrating networks on fibroblast biology, Biomaterials 35 (2014) 8927–8936, doi:10.1016/j.biomaterials.2014.06.047.
- [104] N. Ahmed, C. Riley, G. Rice, M. Quinn, Role of integrin receptors for fibronectin, collagen and laminin in the regulation of ovarian carcinoma functions in response to a matrix microenvironment, Clin. Exp. Metastasis 22 (2005) 391–402, doi:10.1007/s10585-005-1262-y.
- [105] Q. Liu, A. Chiu, L.-H. Wang, D. An, M. Zhong, A.M. Smink, B.J. de Haan, P. de Vos, K. Keane, A. Vegge, E.Y. Chen, W. Song, W.F. Liu, J. Flanders, C. Rescan, L.G. Grunnet, X. Wang, M. Ma, Zwitterionically modified alginates mitigate cellular overgrowth for cell encapsulation, Nat. Commun. 10 (2019) 5262, doi:10.1038/s41467-019-13238-7.
- [106] A. Shikanov, M. Xu, T.K. Woodruff, L.D. Shea, Interpenetrating fibrin-alginate matrices for *in vitro* ovarian follicle development, Biomaterials 30 (2009) 5476–5485, doi:10.1016/j.biomaterials.2009.06.054.
- [107] Z. Guo, T. Zhang, K. Fang, J. Dou, N. Zhou, X. Ma, N. Gu, The effects of macroporosity and stiffness of poly[(methyl vinyl ether)-alt-(maleic acid)] crosslinked egg white simulations of an aged extracellular matrix on the proliferation of ovarian cancer cells, RSC Advances 6 (50) (2016) 43892–43900, doi:10.1039/C6RA05134K.
- [108] D. Loessner, K.S. Stok, M.P. Lutolf, D.W. Hutmacher, J.A. Clements, S.C. Rizzi, Bioengineered 3D platform to explore cell–ECM interactions and drug resistance of epithelial ovarian cancer cells, Biomaterials 31 (32) (2010) 8494– 8506, doi:10.1016/j.biomaterials.2010.07.064.
- [109] T. Zhang, J. Chen, Q. Zhang, J. Dou, N. Gu, Poly(ethylene glycol)-cross linked poly(methyl vinyl ether-co-maleic acid)hydrogels for three-dimensional human ovarian cancer cell culture, Colloids and Surfaces A: Physicochemical and Engineering Aspects 422 (2013) 81–89, doi:10.1016/j.colsurfa.2013.01.030.